Acta Crystallographica Section F
Structural Biology and Crystallization Communications
ISSN 1744-3091

Crystallization and preliminary X-ray analysis of aspartate transcarbamoylase from the parasitic protist *Trypanosoma cruzi*

Kazuaki Matoba,[a] Takeshi Nara,[b] Takashi Aoki,[b] Teruki Honma,[c] Akiko Tanaka,[c] Masayuki Inoue,[d] Shigeru Matsuoka,[d] Daniel Ken Inaoka,[e] Kiyoshi Kita[e] and Shigeharu Harada[a]*

[a]Department of Applied Biology, Graduate School of Science and Technology, Kyoto Institute of Technology, Kyoto 606-8585, Japan, [b]Department of Molecular and Cellular Parasitology, Juntendo University School of Medicine, Tokyo 113-8421, Japan, [c]Systems and Structural Biology Center, RIKEN, Tsurumi, Yokohama 230-0045, Japan, [d]Graduate School of Pharmaceutical Sciences, The University of Tokyo, Tokyo 113-0033, Japan, and [e]Department of Biomedical Chemistry, Graduate School of Medicine, The University of Tokyo, Tokyo 113-0033, Japan

Correspondence e-mail: harada@kit.ac.jp

Received 23 April 2009
Accepted 12 August 2009

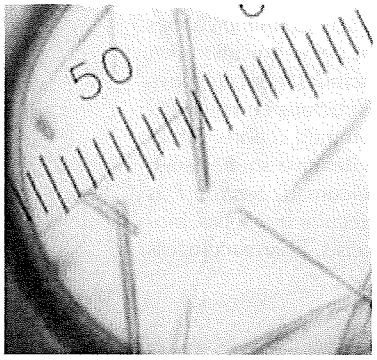

Aspartate transcarbamoylase (ATCase), the second enzyme of the *de novo* pyrimidine-biosynthetic pathway, catalyzes the production of carbamoyl aspartate from carbamoyl phosphate and L-aspartate. In contrast to *Escherichia coli* ATCase and eukaryotic CAD multifunctional fusion enzymes, *Trypanosoma cruzi* ATCase lacks regulatory subunits and is not part of the multifunctional fusion enzyme. Recombinant *T. cruzi* ATCase expressed in *E. coli* was purified and crystallized in a ligand-free form and in a complex with carbamoyl phosphate at 277 K by the sitting-drop vapour-diffusion technique using polyethylene glycol 3350 as a precipitant. Ligand-free crystals (space group $P1$, unit-cell parameters a = 78.42, b = 79.28, c = 92.02 Å, α = 69.56, β = 82.90, γ = 63.25°) diffracted X-rays to 2.8 Å resolution, while those cocrystallized with carbamoyl phosphate (space group $P2_1$, unit-cell parameters a = 88.41, b = 158.38, c = 89.00 Å, β = 119.66°) diffracted to 1.6 Å resolution. The presence of two homotrimers in the asymmetric unit (38 kDa × 6) gives V_M values of 2.3 and 2.5 Å^3 Da^{-1} for the $P1$ and $P2_1$ crystal forms, respectively.

1. Introduction

Chagas disease is a serious tropical disease that is endemic in Central and South America, affecting approximately 16–18 million people in these areas. The causative agent is a flagellate parasitic protist, *Trypanosoma cruzi*, which is transmitted by blood-feeding reduviid bugs. Manifestations of Chagas disease include severe cardiomyopathy, digestive injuries and neural disorders resulting from gradual tissue destruction caused by the parasite. Because nifurtimox and benznidazole, which are the currently used drugs for the treatment of Chagas disease, are toxic and ineffective in the chronic phase, the development of new chemotherapeutic drugs is urgently required (Urbina, 2002).

Pyrimidine biosynthesis is indispensable to all organisms and is achieved *via* the *de novo* and/or salvage pathways. *T. cruzi* possesses both pathways and their balance varies at different developmental stages of the parasite. Since the amastigote stage essentially relies on the *de novo* pathway (Gutteridge & Gaborak, 1979), in which uridine 5′-monophosphate is produced through a series of six enzymatic reactions, the enzymes of the *de novo* pathway therefore provide a greater potential as the primary targets of chemotherapy (Urbina & Docampo, 2003).

Aspartate transcarbamoylase (ATCase; EC 2.1.3.2), the second enzyme of the *de novo* pyrimidine-biosynthetic pathway, catalyzes the production of carbamoyl aspartate from carbamoyl phosphate (CP) and L-aspartate. *Escherichia coli* ATCase is a well known allosteric enzyme and is comprised of catalytic and regulatory subunits, the latter of which carries the binding site of the feedback inhibitor cytidine 5′-triphosphate (CTP; Gerhart & Pardee, 1964; Gerhart & Schachman, 1965; Shepherdson & Pardee, 1960). X-ray structural analysis of the *E. coli* enzyme demonstrated that the enzyme is composed of two trimers of the catalytic subunit (c) and three dimers of the regulatory subunit (r) to form a $(c_3)_2(r_2)_3$ quaternary structure (Krause *et al.*, 1985; Wiley *et al.*, 1972; Wiley & Lipscomb, 1968). ATCases from different strains of *Yersinia enterocolitica* and *Y. enterocolitica*-like organisms also exhibit the $(c_3)_2(r_2)_3$ structure but are sensitive to feedback inhibition by different

pyrimidine nucleotides (Foltermann *et al.*, 1981). *Bacillus subtilis* ATCase lacks the regulatory subunits (Stevens *et al.*, 1991) and in the hyperthermophile *Aquifex aeolicus* six ATCase chains noncovalently associate with six molecules of dihydroorotase (DHO), the third enzyme of the pyrimidine-biosynthetic pathway, to form a dodecamer (Zhang *et al.*, 2009).

On the other hand, eukaryotic ATCases from animals, fungi and Amoebozoa fuse with carbamoyl-phosphate synthetase II (CPS II; the first enzyme of the *de novo* pathway) and DHO to form a multifunctional fusion protein called CAD (Coleman *et al.*, 1977; Freund & Jarry, 1987; Simmer *et al.*, 1989; Souciet *et al.*, 1987), whose feedback inhibitor (CTP) binding site is located in the CPS II domain (Liu *et al.*, 1994). In contrast, *T. cruzi* ATCase (TcATCase), together with the ATCases from plants and other protists, is not part of the CAD multifunctional enzyme and is virtually insensitive to feedback inhibition by pyrimidine nucleotides (Aoki & Oya, 1987) since the enzyme lacks the regulatory subunit (El-Sayed *et al.*, 2005; Gao *et al.*, 1999). In addition, *N*-(phosphonoacetyl)-L-aspartate (PALA), a specific inhibitor of bacterial and mammalian ATCases (Aoki, 1994), only weakly inhibits TcATCase. Thus, structure determination of TcATCase, as well as of the other *de novo* pyrimidine-biosynthetic enzymes of *T. cruzi*, is considered to be crucial for the rational design of chemotherapeutic agents against Chagas disease.

Currently, the crystal structures of bacterial ATCases from *Escherichia coli* (Honzatko *et al.*, 1982), *Bacillus subtilis* (Stevens *et al.*, 1991), *Pyrococcus abyssi* (Van Boxstael *et al.*, 2003), *Sulfolobus acidocaldarius*, *Moritella profunda* (De Vos *et al.*, 2004, 2007) and *Methanococcus jannaschii* (Vitali & Colaneri, 2008), and of the *A. aeolicus* ATCase–DHO complex (Zhang *et al.*, 2009) have been reported. In the present study, we report the expression, purification, crystallization and preliminary X-ray analysis of TcATCase. This is the first crystallization report of an eukaryotic ATCase.

2. Materials and methods

2.1. Preparation of *T. cruzi* ATCase

The *T. cruzi* ATCase genes were previously cloned by screening the total DNA library of *T. cruzi* Tulahuen strain (Nara *et al.*, 2003). *T. cruzi* Tulahuen possesses three copies of the ATCase gene (*tcact1*, *tcact2* and *tcact3*, with GenBank accession Nos. AB074138, AB074139 and AB074140, respectively) and *tcact2* was selected for expression. The open reading frame of *tcact2* was amplified by PCR using 5′-CGGGATCCATGTTGGAACTGCCGCCAG-3′ and 5′-CGGGATCCTCACGCCAAAACGCTCCAC-3′ as the forward and reverse primers, respectively, and then subcloned into the bacterial expression vector pET14b (Novagen, EMD Biosciences Inc., Madison, Wisconsin, USA). The recombinant plasmid was introduced into *E. coli* BL21 (DE3) pLysS (Novagen). The transformant was grown in 1000 ml Luria–Bertani medium containing 50 µg ml^{-1} carbenicillin at 310 K until the absorbance at 600 nm (A_{600}) reached about 0.6. Expression of the recombinant His$_6$-tagged TcATCase was induced with 1 m*M* isopropyl β-D-1-thiogalactopyranoside at 310 K for 2 h. The cells were harvested by centrifugation at 5000*g* for 10 min and suspended in 20 ml lysis buffer (20 m*M* Tris–HCl pH 8.0, 0.5 *M* NaCl, 40 m*M* imidazole). After disruption of the cells by sonication, the lysate was centrifuged at 15 000*g* at 277 K for 20 min. The supernatant containing the His$_6$-tagged TcATCase was filtrated with a 0.22 µm pore-size filter and loaded onto a His-Trap FF column (1 ml bed volume; GE Healthcare) pre-equilibrated with lysis buffer. The column was then washed with 20 ml lysis buffer and the bound His$_6$-tagged TcATCase was eluted from the column with lysis buffer containing 500 m*M* imidazole. The fractions containing TcATCase were pooled and the buffer was exchanged to 20 m*M* Tris–HCl pH 7.4 using a PD-10 desalting column (GE Healthcare); they were then concentrated to 10 mg ml^{-1} with a centrifugal concentrator tube (Amicon Ultra-4 Ultracel-10K).

The ATCase activity was assayed by monitoring the production of carbamoyl aspartate from CP and L-aspartate by Ceriotti's colorimetric method (Prescott & Jones, 1969) with minor modifications. Briefly, 0.5 ml of a reaction mixture containing 200 m*M* Tris–HCl pH 7.9, 30 m*M* L-aspartate and purified ATCase was pre-incubated in a 1.5 ml quartz cuvette at 310 K for 5 min and the enzymatic reaction was then started by adding CP to a final concentration of 1.3 m*M*. CP was dissolved in ice-cold distilled water just before measurement. After standing for 15 min at 310 K, the reaction was stopped and 0.5 ml of a 1:1 mixture of 0.5% antipyrine in 50% sulfonic acid and 0.8% diacetylmonoxime in 5% acetic acid was added. Colorimetric development of the diazine produced from the carbamoyl aspartate and diacetylmonoxime was performed at 333 K for 2 h in the dark and the A_{466} was measured. The concentration of the carbamoyl aspartate produced was estimated from the A_{466} values of standard solutions containing carbamoyl aspartate at known concentrations. The typical specific activity of the purified TcATCase was 9 µmol min^{-1} mg^{-1} and the K_m values for CP and L-aspartate were estimated to be 0.03 and 29.4 m*M*, respectively.

TcATCase was purified to apparent homogeneity as shown by SDS–PAGE (Fig. 1), with a yield of about 2 mg from a 1000 ml culture. Gel-filtration chromatography with TSK-gel G3000SWXL (7.8 × 300 mm, Tosoh) and dynamic light-scattering analysis using DynaPro Titan (Wyatt Technology) both indicated that the purified enzyme existed as a homotrimer in solution.

2.2. Crystallization and X-ray data collection

All crystallization experiments were performed by the sitting-drop vapour-diffusion technique in 96-well Corning CrystalEX micro-

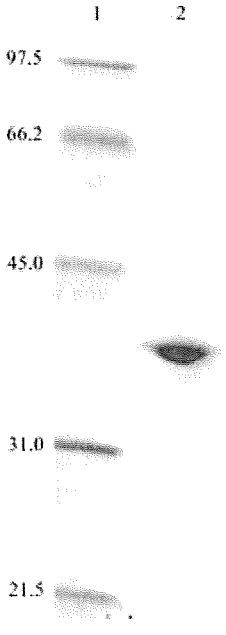

Figure 1
12.5% SDS–PAGE gel stained with Coomassie Brilliant Blue R-250 showing the apparent homogeneity of the purified TcATCase. Lane 1, molecular-weight markers (kDa); lane 2, TcATCase purified using a His-Trap FF column.

Table 1
Statistics of data collection and processing.

Values in parentheses are for the highest resolution shell.

	Ligand-free TcATCase	TcATCase–CP complex
Wavelength (Å)	0.900 (SPring-8 BL44XU)	1.000 (SPring-8 BL41XU)
Space group	$P1$	$P2_1$
Unit-cell parameters (Å, °)	a = 78.42, b = 79.28, c = 92.02, α = 69.56, β = 82.90, γ = 63.25	a = 88.41, b = 158.38, c = 89.00, β = 119.66
Solvent content† (%)	48	51
Frame number	222	180
Resolution range (Å)	50.0–2.8 (2.90–2.80)	50.0–1.60 (1.66–1.60)
No. of reflections	103124	946629
Unique reflections	44850	277190
Mosaicity	0.90	0.21
Redundancy	2.3 (2.3)	3.4 (3.4)
Completeness (%)	97.7 (98.4)	95.3 (91.4)
R_{merge}‡ (%)	7.4 (38.9)	6.5 (39.9)
Mean $I/\sigma(I)$	15.8 (4.4)	11.7 (3.9)

† Assuming the presence of six molecules in the asymmetric unit. ‡ $R_{merge} = \sum_{hkl}\sum_i |I_i(hkl) - \langle I(hkl)\rangle| / \sum_{hkl}\sum_i I_i(hkl)$, where $I_i(hkl)$ is the intensity of the ith observation of reflection hkl.

plates with a conical flat bottom (Hampton Research). In the initial screening for crystallization conditions, a 0.5 µl droplet containing around 10 mg ml^{-1} TcATCase dissolved in 20 mM Tris–HCl pH 7.4 was mixed with an equal volume of reservoir solution and the droplet was allowed to equilibrate against 100 µl reservoir solution at 277 and 293 K. Commercially available screening kits purchased from Hampton Research (Crystal Screen, Crystal Screen 2, Crystal Screen Lite and SaltRx) and Emerald BioStructures (Wizard I, Wizard II, Cryo I and Cryo II) were used as reservoir solutions. Of the 434 conditions screened, condition No. 10 from Crystal Screen Lite [15%(*w*/*v*) PEG 4000, 0.1 *M* sodium acetate pH 4.6, 0.2 *M* ammonium acetate] gave tiny plate-shaped crystals at 277 K. The condition was then optimized using 154 conditions by varying the PEG concentration (4–16%), the buffer pH (3.6–5.6) and the temperature (277 and 293 K) using PEG 3350, which is a monodisperse and high-purity polyethylene glycol obtained from Hampton Research, as a precipitant. For the best condition found, the effects of 72 additives on crystallization were examined using Additive Screen kits (Hampton Research) according to the manufacturer's instruction. Cobalt chloride and glycerol improved the size of the crystals; moreover, the addition of both additives gave thicker crystals. Currently, crystals larger than 0.2 × 0.1 × 0.01 mm can be grown at 277 K from reservoir solution containing 8–10%(*w*/*v*) PEG 3350, 0.1 *M* acetate buffer pH 4.6, 0.2 *M* ammonium acetate, 0.01 *M* cobalt chloride and 3% glycerol. For cocrystallization with CP, a freshly prepared 100 m*M* CP solution was added to the TcATCase solution to give a final concentration of 5 m*M* and crystallization was conducted as described above. Crystals of similar shape and size were obtained.

X-ray diffraction experiments were performed on the BL44XU beamline (λ = 0.900 Å; equipped with a Bruker DIP-6040 detector system) and the BL41XU beamline (λ = 1.000 Å; equipped with a Rayonix CCD MX225HE detector) at SPring-8 (Harima, Japan) and on the BL17A beamline (λ = 1.000 Å; equipped with an ADSC Quantum 270 detector) at Photon Factory (Tsukuba, Japan). A crystal mounted in a nylon loop was transferred and soaked briefly in reservoir solution supplemented with 20%(*w*/*v*) glycerol and then flash-cooled by rapidly submerging it in liquid nitrogen. Diffraction data were collected under cryocooled conditions at 100 K. Images were recorded with an oscillation angle of 1°, an exposure time of 1 s per frame and a crystal-to-detector distance of 150 mm and were processed with the *HKL*-2000 software package (Otwinowski & Minor, 1997).

3. Results and discussion

His_6-tagged TcATCase (38 kDa) could be purified to homogeneity by one-step purification using His-Trap FF column chromatography (Fig. 1). The molecular weight of the purified enzyme estimated by gel-filtration chromatography (134 kDa) and dynamic light scattering (102 kDa; R_h = 4.3 nm, polydispersity = 13.9%, mass = 100%) indicated that the enzyme probably exists as a homotrimer in solution.

Crystals of ligand-free TcATCase were obtained at 277 K from reservoir solution containing 8–10%(*w*/*v*) PEG 3350, 0.1 *M* acetate buffer pH 4.6, 0.2 *M* ammonium acetate, 0.01 *M* cobalt chloride and 3% glycerol and reached maximum dimensions within two weeks (Fig. 2*a*). TcATCase complexed with CP was also crystallized by the cocrystallization method under the same conditions within 2 d (Fig. 2*b*). Analyses of the symmetry and systematic absences in the recorded diffraction patterns indicated that the crystals of ligand-free TcATCase belonged to the triclinic space group $P1$, with unit-cell parameters a = 78.42, b = 79.28, c = 92.02 Å, α = 69.56, β = 82.90, γ = 63.25°, whereas those of TcATCase complexed with CP belonged to the monoclinic space group $P2_1$, with unit-cell parameters a = 88.41, b = 158.38, c = 89.00 Å, β = 119.66°. Assuming the presence of two His_6-tagged TcATCase trimers (6 × 38 kDa) in the asymmetric unit, the V_M values are 2.3 and 2.5 Å^3 Da^{-1} for the triclinic and monoclinic

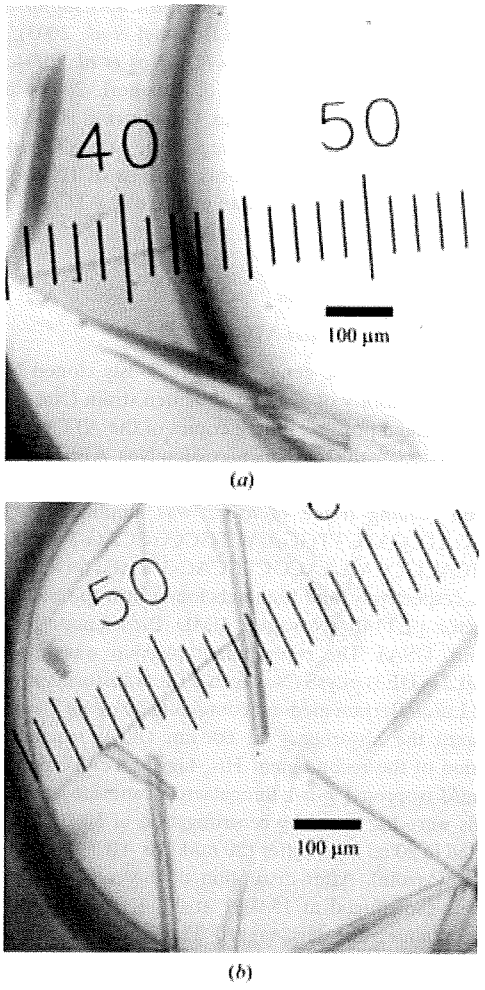

Figure 2
Crystals of (*a*) ligand-free TcATCase and (*b*) TcATCase complexed with carbamoyl phosphate obtained by the sitting-drop vapour-diffusion method using PEG 3350 as a precipitant.

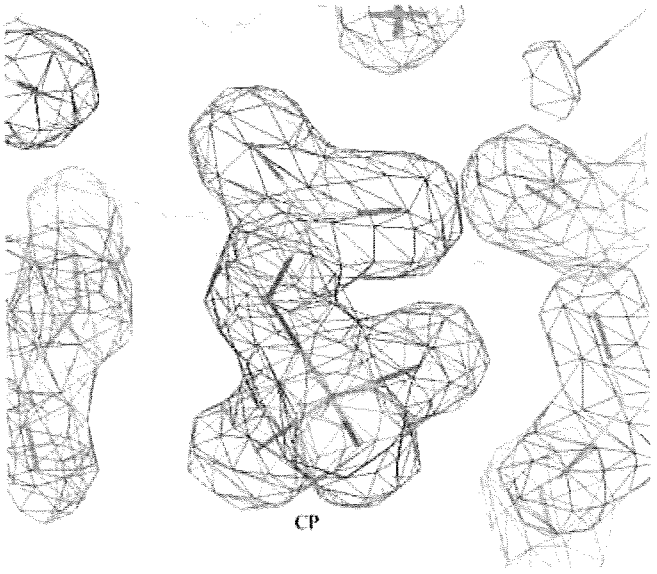

Figure 3
The $2F_o - F_c$ electron-density map around the bound CP in the TcATCase–CP complex structure contoured at 2σ. The structure is currently refined to $R = 0.151$ (1.6 Å resolution).

crystal forms, respectively; these values are within the range commonly observed for protein crystals (Matthews, 1968). A data set to 2.8 Å resolution (44 850 unique reflections) was obtained for ligand-free TcATCase after merging 103 124 reflections recorded on 222 images, while 277 190 unique reflections to 1.6 Å resolution were produced from 946 629 measured reflections on 180 images for TcATCase complexed with CP. Statistics of data collection and processing are shown in Table 1.

Attempts to solve the structures of both crystal forms by the molecular-replacement method with the *MOLREP* program (Vagin & Teplyakov, 1997) as implemented within the *CCP*4 package (Collaborative Computational Project, Number 4, 1994) were carried out using the homotrimeric structure of the catalytic subunit of *P. abyssi* ATCase (PDB code 1ml4; 40.1% amino-acid sequence identity with TcATCase), which showed a higher identity to TcATCase than to the ATCases from *E. coli* (PDB code 2atc; 36.5% identity), *B. subtilis* (PDB code 2at2; 32.5% identity), *S. acidocaldarius* (PDB code 2be9; 36.8% identity), *Moritella profunda* (PDB code 2be7; 37.7% identity), *Methanococcus jannaschii* (PDB code 2rgw; 38.6% identity) and *A. aeolicus* (PDB code 3d6n; 21.2% identity). A promising solution with two homotrimers per asymmetric unit was obtained for both the ligand-free TcATCase (correlation coefficient and R factor of 0.551 and 49.0%, respectively) and the TcATCase–CP complex (correlation coefficient and R factor of 0.615 and 50.9%, respectively). The models were subsequently subjected to rigid-body refinement and gave R factors of 44.8% and 44.4% for ligand-free TcATCase and the TcATCase–CP complex, respectively. Refinement of the structures is currently in the final stages. Clear electron densities for the entire protein part and the bound CP were observed for the TcATCase–CP complex (Fig. 3), but the loop of the CP-binding site (Cys85–Thr95) was disordered in the ligand-free TcATCase. The suppression of the flexibility of the loop by the bound CP may lead to the different crystal form and the enhanced X-ray diffraction of the crystals of the TcATCase–CP complex. We are now trying to prepare crystals of TcATCase complexed with potential inhibitors found in the Chemical Library of the Chemical Biology Research Initiative, University of Tokyo by *in silico* screening. Since the enzymes of the *de novo* pyrimidine-biosynthetic pathway have great potential as primary targets of chemotherapy (Urbina & Docampo, 2003), the detailed structures of TcATCase complexed with these compounds will help in structure-based drug design aimed at Chagas disease.

We thank all staff members of beamlines BL41XU and BL44XU at SPring-8 and BL17A at Photon Factory for their help with the X-ray diffraction experiments. This work was supported by a grant from the Targeted Proteins Research Program (TPRP) and was supported in part by a grant-in-aid for Creative Scientific Research (18GS0314 to KK) from the Japan Society for the Promotion of Science and a grant-in-aid for Scientific Research on Priority Areas (18073004) from the Japanese Ministry of Education, Science, Culture, Sports and Technology.

References

Aoki, T. (1994). *Jpn. J. Parasitol.* **43**, 1–10.
Aoki, T. & Oya, H. (1987). *Comput. Biochem. Physiol. B*, **87**, 143–150.
Coleman, P. F., Suttle, D. P. & Stark, G. R. (1977). *J. Biol. Chem.* **252**, 6379–6385.
Collaborative Computational Project, Number 4 (1994). *Acta Cryst.* D**50**, 760–763.
De Vos, D., Van Petegem, F., Remaut, H., Legrain, C., Glansdorff, N. & Van Beeumen, J. J. (2004). *J. Mol. Biol.* **339**, 887–900.
De Vos, D., Xu, Y., Hulpiau, P., Vergauwen, B. & Van Beeumen, J. J. (2007). *J. Mol. Biol.* **365**, 379–395.
El-Sayed, N. M. *et al.* (2005). *Science*, **309**, 409–415.
Foltermann, K. F., Wild, J. R., Zink, D. L. & O'Donovan, G. A. (1981). *Curr. Microbiol.* **6**, 43–47.
Freund, J. N. & Jarry, B. P. (1987). *J. Mol. Biol.* **193**, 1–13.
Gao, G., Nara, T., Nakajima-Shimada, J. & Aoki, T. (1999). *J. Mol. Biol.* **285**, 149–161.
Gerhart, J. C. & Pardee, A. B. (1964). *Fed. Proc.* **23**, 727–735.
Gerhart, J. C. & Schachman, H. K. (1965). *Biochemistry*, **4**, 1054–1062.
Gutteridge, W. E. & Gaborak, M. (1979). *Int. J. Biochem.* **10**, 415–422.
Honzatko, R. B., Crawford, J. L., Monaco, H. L., Ladner, J. E., Ewards, B. F., Evans, D. R., Warren, S. G., Wiley, D. C., Ladner, R. C. & Lipscomb, W. N. (1982). *J. Mol. Biol.* **160**, 219–263.
Krause, K. L., Volz, K. W. & Lipscomb, W. N. (1985). *Proc. Natl Acad. Sci. USA*, **82**, 1643–1647.
Liu, X., Guy, H. I. & Evans, D. R. (1994). *J. Biol. Chem.* **269**, 27747–27755.
Matthews, B. W. (1968). *J. Mol. Biol.* **33**, 491–497.
Nara, T., Hirayama-Noguchi, Y., Gao, G., Murai, E., Annoura, T. & Aoki, T. (2003). *Int. J. Parasitol.* **33**, 845–852.
Otwinowski, Z. & Minor, W. (1997). *Methods Enzymol.* **276**, 307–326.
Prescott, L. M. & Jones, M. E. (1969). *Anal. Biochem.* **32**, 408–419.
Shepherdson, M. & Pardee, A. B. (1960). *J. Biol. Chem.* **235**, 3233–3237.
Simmer, J. P., Kelly, R. E., Scully, J. L., Grayson, D. R., Rinker, A. G. Jr, Bergh, S. T. & Evans, D. R. (1989). *Proc. Natl Acad. Sci. USA*, **86**, 4382–4386.
Souciet, J. L., Potier, S., Hubert, J. C. & Lacroute, F. (1987). *Mol. Gen. Genet.* **207**, 314–319.
Stevens, R. C., Reinisch, K. M. & Lipscomb, W. N. (1991). *Proc. Natl Acad. Sci. USA*, **88**, 6087–6091.
Urbina, J. A. (2002). *Curr. Pharm. Des.* **8**, 287–295.
Urbina, J. A. & Docampo, R. (2003). *Trends Parasitol.* **19**, 495–501.
Vagin, A. & Teplyakov, A. (1997). *J. Appl. Cryst.* **30**, 1022–1025.
Van Boxstael, S., Cunin, R., Khan, S. & Maes, D. (2003). *J. Mol. Biol.* **326**, 203–216.
Vitali, J. & Colaneri, M. J. (2008). *Acta Cryst.* F**64**, 776–780.
Wiley, D. C., Evans, D. R., Warren, S. G., McMurray, C. H., Edwards, B. F., Franks, W. A. & Lipscomb, W. N. (1972). *Cold Spring Harb. Symp Quant. Biol.* **36**, 285–290.
Wiley, D. C. & Lipscomb, W. N. (1968). *Nature (London)*, **218**, 1119–1121.
Zhang, P., Martin, P. D., Purcarea, C., Vaishnav, A., Brunzelle, J. S., Fernando, R., Guy-Evans, H. I., Evans, D. R. & Edwards, B. F. (2009). *Biochemistry*, **48**, 766–778.

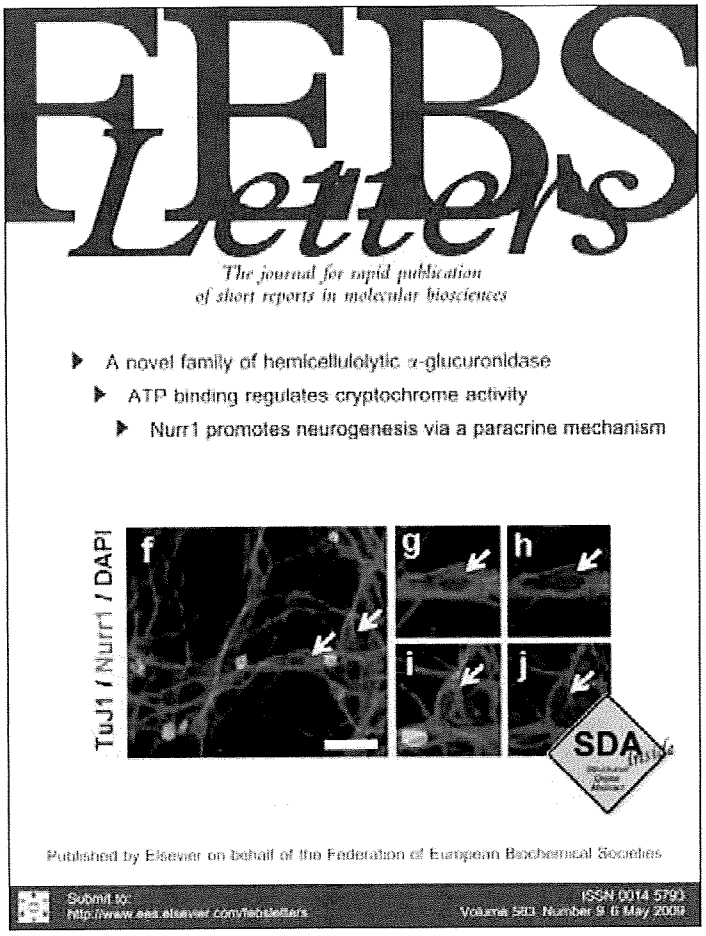

FEBS Letters 583 (2009) 1446–1450

FEBS Letters

journal homepage: www.FEBSLetters.org

The *Plasmodium* HU homolog, which binds the plastid DNA sequence-independent manner, is essential for the parasite's survival

Narie Sasaki [a,b], Makoto Hirai [c], Katsura Maeda [b], Ryoko Yui [a], Kie Itoh [d], Syoko Namiki [a], Teppei Morita [a], Masayuki Hata [e], Kimiko Murakami-Murofushi [b], Hiroyuki Matsuoka [c], Kiyoshi Kita [e], Shigeharu Sato [f,*]

[a] *Division of Biological Science, Graduate School of Science, Nagoya University, Nagoya 464-8602, Japan*
[b] *Department of Biology, Faculty of Science, Ochanomizu University, Tokyo 112-0012, Japan*
[c] *Division of Medical Zoology, Department of Infection and Immunity, Jichi Medical University School of Medicine, Shimotsuke 329-0498, Japan*
[d] *Department of Integrated Biosciences, Graduate School of Frontier Sciences, University of Tokyo, 5-1-5 Kashiwanoha, Kashiwa 277-8562, Japan*
[e] *Department of Biomedical Chemistry, Graduate School of Medicine, The University of Tokyo, Tokyo 113-0033, Japan*
[f] *Division of Parasitology, MRC National Institute for Medical Research, London NW7 1AA, UK*

ARTICLE INFO

Article history:
Received 27 February 2009
Revised 26 March 2009
Accepted 31 March 2009
Available online 7 April 2009

Edited by Michael Ibba

Keywords:
DNA binding protein
HU
Knock-out
Plastid
Plasmodium berghei
Plasmodium falciparum

ABSTRACT

The nuclear genome of the human malaria parasite *Plasmodium falciparum* encodes a homolog of the bacterial HU protein (PfHU). In this study, we characterised PfHU's physiological function. PfHU, which is targeted exclusively to the parasite's plastid, bound its natural target – the plastid DNA – sequence-independently and complemented lack of HU in *Escherichia coli*. The HU gene could not be knocked-out from the genome of *Plasmodium berghei*, implying that HU is important for the parasite's survival. As the human cell lacks the HU homolog, PfHU is a potential target for drugs to control malaria.

1. Introduction

Apicomplexan parasites such as the human malaria parasite *Plasmodium falciparum* have a vestigial secondary plastid that is often called the apicoplast [1]. Despite being non-photosynthetic, the apicomplexan plastid is indispensable for the parasite because the organelle is involved in essential metabolism such as isoprenoid biosynthesis [2]. The *P. falciparum* plastid contains its own genomic DNA which is 35 kb in size and extremely rich in A + T (86%) [1]. Almost all proteins encoded by the plastid DNA (ptDNA) are involved in either transcription or translation. Nevertheless, the plastid genome encodes at least one gene whose expression is critical for the parasite's survival, and drugs affecting bacterial type gene expression often cause the delayed death phenotype of the parasite [3].

In the plastid, genomic DNA is assembled into a compact, highly organised structure, the nucleoid [4], like in bacteria from which the plastid has evolved. Bacterial nucleoid formation depends on a group of bacterial histone-like DNA binding proteins (BHLs). The HU protein, which binds DNA in a sequence non-specific manner and bends the bound DNA, is the most abundant BHL in the bacterial cell [5]. *Escherichia coli* HU is a heterodimer of two highly homologous subunits HUα and HUβ, which are encoded by *hupA* and *hupB*, respectively [6]. HU is ubiquitously distributed among bacteria and this suggests that the protein is critical in bacterial nucleoid formation. In addition to an architectural role, HU is also involved in other cellular functions such as initiation of replication [7], transcriptional regulation [8] and DNA recombination [9] in *E. coli*.

Although the plastids of the photosynthetic eukaryotes are descendents of bacteria, their original, bacterial components have been gradually replaced to eukaryotic factors of equivalent function during the course of evolution. Today, the plastid HU homolog is only found in some algal species and apicomplexans [4]. The algal HUs such as those of *Cyanidioschyzon merolae* [10] and *Guillardia theta* [11] are capable of rescuing bacterial HU null mutants

Abbreviations: BHL, bacterial histone-like DNA binding protein; ptDNA, plastid DNA

* Corresponding author. Fax: +44 20 8816 2730.
E-mail address: ssato@nimr.mrc.ac.uk (S. Sato).

0014-5793/$36.00
doi:10.1016/j.febslet.2009.03.071

from its abnormal phenotype. The HU of *G. theta* bends DNA to which it binds [11], suggesting that this protein is critical in the formation of the nucleoid in this alga's plastid.

Recently, Ram et al. reported that the nuclear genome of *P. falciparum* encodes a HU homolog (PfHU) that is probably involved in DNA compaction in the plastid [12]. They found PfHU doesn't exhibit the DNA-bending activity in vitro and attributed this to the fact that the protein lacks the highly conserved proline residue at the position corresponding to P63 of *E. coli* HUα.

In this study, we investigated how PfHU binds the plastid DNA, whether the protein complements lack of HU in an *E. coli* null mutant, and whether HU protein is essential in the related rodent malaria parasite *P. berghei*, in order to characterise the physiological function of PfHU.

2. Materials and methods

2.1. DNA-mobility shift assay

The Recombinant PfHUs, PfHU53-189 and PfHU53-148 were prepared as described in Supplementary material. DNA fragments A1280, A1838, B1624 and B1880 were PCR-amplified from the parasite's ptDNA with a set of synthetic primers described by Singh et al. [13]; AB1677 was amplified with 5′-CTTTATATGGAGCTCGTCCT-3′ and 5′-CTGATTTATTACCTGTTGGT-3′. Fifty nanograms of each DNA fragment was incubated with each recombinant protein (0, 50, 100, 200, 400, and 800 ng) in the reaction buffer (20 mM Tris–HCl, pH 7.5, 0.4 mM EDTA, 20 mM NaCl, 0.4 mM DTT) for 3 h at room temperature before application to a 1% agarose gel and electrophoresis, then the gel was stained with ethidium bromide.

2.2. Complementation test

The *hupB*::Km^r locus of the HUβ$^-$ *E. coli* strain JR1671 was transduced to the HUα$^-$ strain JR1670 carrying *hupA*::Cm^r to generate a *hupAhupB* double mutant by P1 transduction [14]. A pQE50 (Qiagen)-base expression plasmid encoding PfHU53-189 without an affinity tag was constructed and the *hupAhupB* double mutant was transformed with a plasmid expressing the recombinant protein. The transformant was grown on LB supplemented with 50 μg/ml kanamycin and 50 μg/ml ampicillin. Neither chloramphenicol nor IPTG was added to the growth medium because the double mutant was sensitive to chroramphenicol [14] and the excess induction of PfHU53-189 was harmful for growth of the bacteria (data not shown).

2.3. Knock-out of the nuclear gene of Plasmodium berghei

To disrupt the HU gene of *P. berghei* (PB000792.02.0) through double-crossover homologous recombination, the plasmid pPbHU-KO was constructed from pBS-DHFR [15] following the method used to construct another targeting plasmid pPbGCS1-KO, which was successfully used to knock-out the GCS1 gene of the parasite [16] (details in Supplementary material). *P. berghei* ANKA clone 2.34 was separately transfected with pPbGCS1-KO or pPbHU-KO by electroporation, and recombinant parasites were selected with pyrimethamine.

3. Results

3.1. PfHU binds the plastid DNA sequence-independently

Ram and colleagues reported that PfHU exhibits the DNA binding activity that is predictable from the presence of a complete BHL domain in the protein [12]. They also reported that PfHU is localised to the plastid [12]. We confirmed the plastid-specific location of the protein by immuno-fluorescence microscopy using the anti-PfHU antibody (Supplementary Fig. S1). Therefore, the organellar genomic DNA in the plastid is the only natural target of the binding of PfHU. Ram and colleagues carried out chromatin immuno-precipitation (ChIP) assays and suggested that PfHU binds at least part of the organellar DNA [12], but no further analysis has been done. Thus, in order to characterise the physiological function of PfHU in detail, we analysed the protein's binding to different parts of the ptDNA by DNA-mobility shift assay using the recombinant protein.

Transfection experiments using yellow fluorescent protein (YFP) fused to Met1-Met82 of PfHU (PfHU-YFP) showed that the N-terminal sequence functions as the plastid targeting sequence (Supplementary Fig. S2). We prepared two differently truncated forms of the recombinant PfHU, PfHU53-189 and PfHU53-148; PfHU53-189 lacks the N-terminal unconserved sequence (M1-I52) whereas PfHU53-148 contains only the BHL domain (Fig. 1A). The apparent molecular mass of PfHU53-189 determined by Western blotting is almost the same as the natural PfHU present in the parasite (Supplementary Fig. S3). This suggests that the unconserved N-terminal sequence is removed from the mature form of PfHU, which is almost the same as PfHU53-189, when the protein is targeted to the plastid.

For this analysis, we selected five different regions of the ptDNA (Fig. 1B). Four of them – A1838, A1820, B1624 and B1880 – were chosen from those described in the previous report by Singh et al [13], as they are in close proximity of the DNA replication initiation sites (A1820), protein coding regions with tRNA genes' cluster (B1624 and B1880) and a part of a protein coding gene (A1838), respectively. In addition, another region AB1677, which contains the ends of both the two gene clusters, was selected as it is supposed to be important in termination of transcription.

A PCR fragment of each region was incubated with PfHU53-189 and separated by agarose gel electrophoresis (Fig. 1C). The result clearly showed that the protein affected the mobility of all the five fragments. Shift of the band was apparent even at a protein/DNA mass ratio = 1 but it was much more prominent when the ratio was higher. The protein added at the same mass ratio affected the mobility of each fragment equally. This indicates that PfHU53-189 binds these five DNA fragments regardless of their size and nucleotide sequence. This suggests that PfHU binds the ptDNA sequence without specificity.

Another experiment with PfHU53-148, which consists of only the BHL domain of PfHU, showed that this shorter form also binds the ptDNA sequence-independently, though the protein's affinity for each fragment seemed to be lower than that of PfHU53-189 (Fig. 1D). This implies that the BHL domain is sufficient for PfHU to bind the DNA and the unique C-terminal sequence stabilises the DNA–protein complex.

3.2. PfHU complements the HU-deficient E. coli mutant

Although neither of the two genes (*hupA* and *hupB*) encoding the two subunits of HU is essential for the survival of *E. coli* on LB at 37 °C, *hupAhupB* double mutants exhibit characteristic phenotypes such as filamentous morphology and sensitivity to the cold [17]. To characterise the function of PfHU further, a *hupAhupB* double mutant strain was transformed with the expression plasmid for PfHU53-189 and the effect of the expressed recombinant protein on the mutant's phenotypes investigated.

Unlike the HU$^+$ parent strain JR1669 that is short and homogeneous in size, the *hupAhupB* double mutant exhibits a characteristic filamentous phenotype (Fig. 2A). On the LB plate, the mutant forms visible colonies at 37 °C, but no visible colony is formed at 25 °C (Fig. 2B). By contrast, the transformants expressing

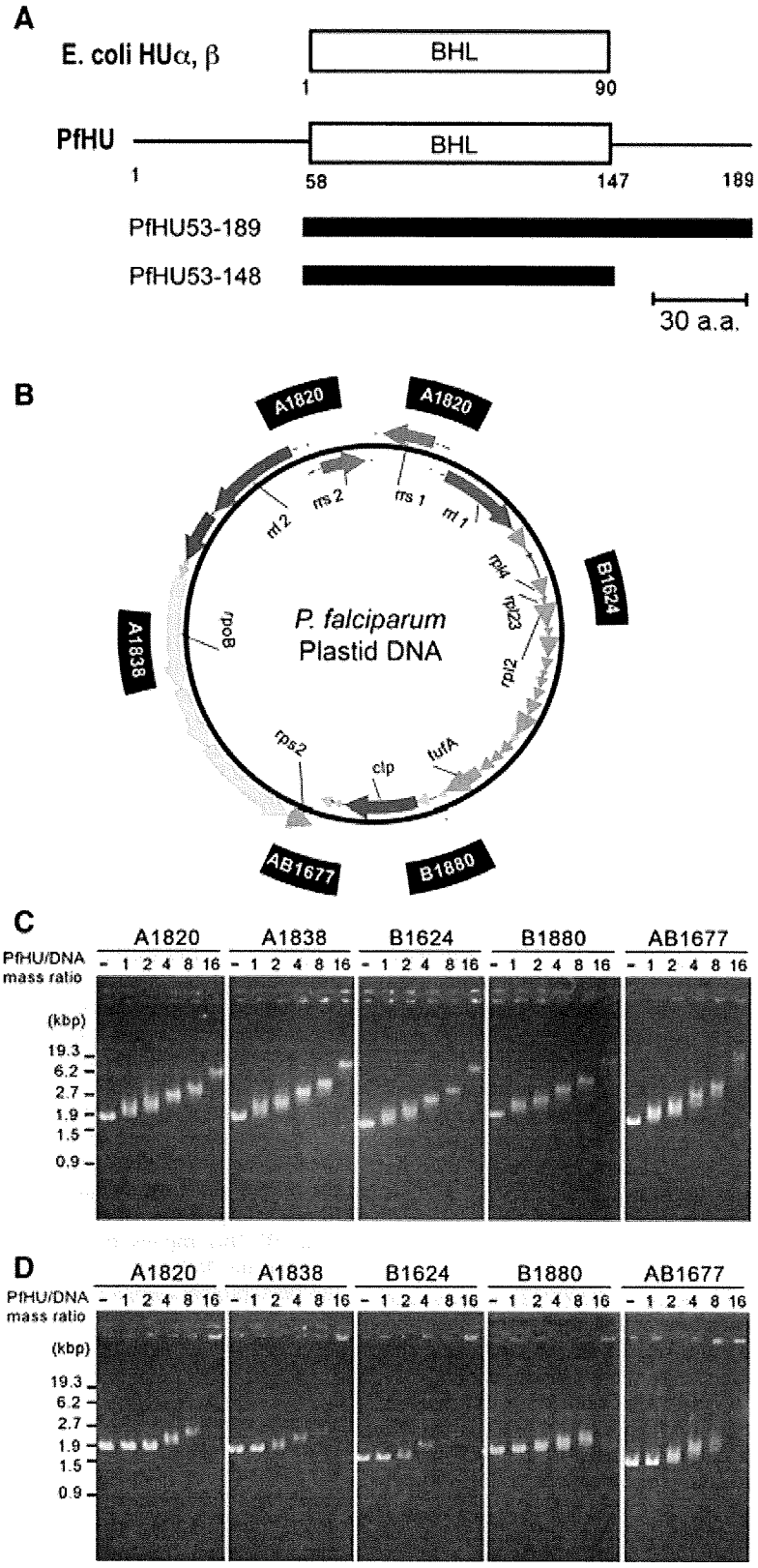

Fig. 1. PfHU binds the plastid DNA sequence-independently. (A) PfHU and its two recombinant forms. The BHL domain corresponding to the *E. coli* HU subunits is boxed. (B) Map of the plastid DNA of *P. falciparum*. The position of each DNA fragment used in the DNA-mobility shift assay is indicated outside the map. (C and D) DNA mobility shift assay. C, PfHU53-189; D, PfHU53-148. Note that the mobility of all fragments tested was similarly affected by each recombinant PfHU. The number of base pairs per one molecule of PfHU is 26 (PfHU53-189) or 18 (PfHU53-148), when the mass ratio of the protein to DNA is 1.

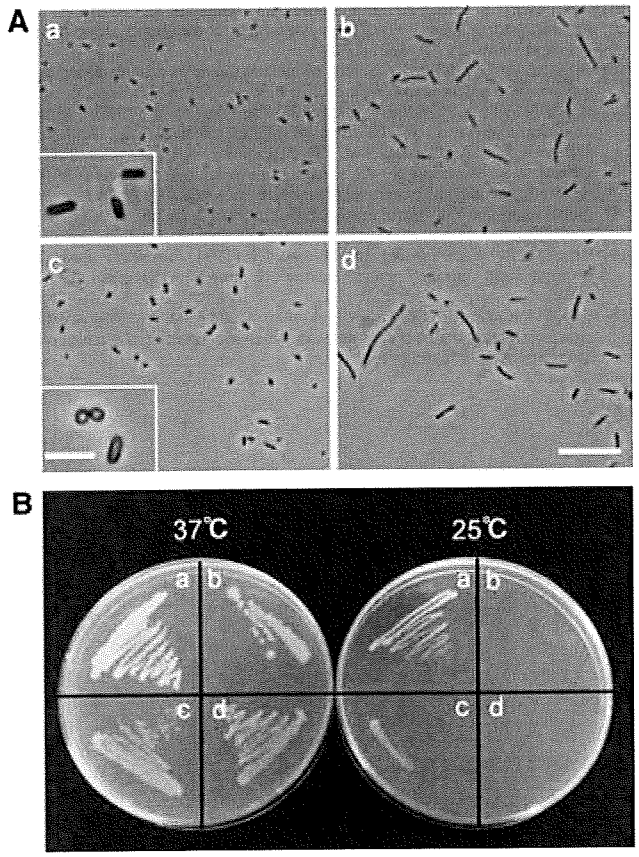

Fig. 2. PfHU complements the lack of HU in *E. coli*. (A) Phase-contrast micrographs of the HU$^+$ strain (a), the *hupAhupB* mutant (b), the *hupAhupB* mutant expressing PfHU53-189 (c) and the *hupAhupB* mutant carrying pQE50 (d). Scale bar: 5 μm. Inset, magnified view. Scale bar: 1 μm. (B) Growth of bacteria on LB plate at different temperature. Bacteria in each sector (a–d) were as in A. Each plate was incubated for 20 h (37 °C) or 40 h (25 °C).

PfHU53-189 were short in length and looked similar to the HU$^+$ parent strain (Fig 2Ac), and capable of forming robust colonies on the LB plate at both the permissive (37 °C) and the restrictive (25 °C) temperatures (Fig. 2B). The presence of the expression vector itself did not affect either the filamentous- or the cold-sensitive-phenotype of the double mutant. These results suggest that the PfHU53-189 functionally complements the deficiency of HU of the *hupAhupB* strain.

3.3. The HU gene is important for survival of the malaria parasite

Not only *P. falciparum* but other *Plasmodium* spp. have one gene for HU in the nuclear genome; for example, PB000792.02.0 (*PbHU*) is the gene of the rodent malaria parasite *P. berghei*. *Plasmodium* HUs are closely related to each other and the sequence alignment suggests that each *Plasmodium* HU has a plastid targeting sequence at the N terminus (Supplementary Fig. S4). This implies that all these *Plasmodium* HUs share the same physiological function(s). To investigate the importance of HU for *Plasmodium* spp., we constructed a targeting plasmid pPbHU-KO from pBS-DHFR [15] and attempted to disrupt the *HU* gene of *P. berghei* with the plasmid. Although the control experiment with a sister pBS-DHFR-based plasmid pPbGCS1-KO [16] easily generated the *PbGCS1* gene disruptant, we never obtained the *PbHU* knockout parasite in several repeated trials. This suggests that the *PbHU* locus is essential for the parasite's survival at least during the asexual blood stage, and that the gene is also indispensible for the survival of other species such as *P. falciparum*. Probably the HU protein encoded by the gene is important for the function and/or maintenance of the ptDNA of *Plasmodium* spp., though another possibility that the manipulation of this particular locus adversely affects the expression of other important genes [18] has not been ruled out yet.

4. Discussion

PfHU is a plastid protein and our mobility shift assay confirmed that PfHU's direct binding to the parasite's ptDNA is sequence-independent. These data imply that PfHU is involved in the assembly of the nucleoid in the plastid as an architectural protein. The filamentous phenotype of the *E. coli hupAhupB* mutant is attributed to perturbed expression of specific cell division genes [19] whereas the cold-sensitive phenotype of the mutant can be caused by unstable binding of DnaA to the binding sites in the chromosomal replication origin *oriC* [6,20]. Thus, data obtained by our complementation test suggest that PfHU adjusted the expression of genes determining bacterial shape and promoted initiation of chromosome replication by stabilising DnaA's binding to *oriC* in *E. coli*. It is questionable whether the *Plasmodium* plastid and *E. coli* share the same regulation systems for either gene expression or chromosome replication, but our data suggest that PfHU is capable to exhibits sequence-specific functions presumably by changing the architectural structure of ptDNA in the plastid.

The HU gene was impossible to knock-out from the genome of *P. berghei*, strongly suggesting that the *HU* gene is also likely indispensible for the survival of *P. falciparum*. Although it is hardly known how gene expression and replication of the organellar DNA are regulated in the *Plasmodium* plastid, PfHU is possibly involved in such sequence-dependent events in addition to general maintenance of ptDNA. Because a HU ortholog is absent from the humans, PfHU should be a promising target of the controlling drugs against malaria.

Acknowledgements

The authors thank Dr. J. Rouviere-Yaniv (Institut Pasteur, France) for providing us with *E. coli* strains JR1669, JR1670 and JR1671. This work was financially supported by the British Medical Research Council (MRC), and a Grant-in-Aid for Creative Scientific Research (18GS0314-01 to N.S. and 18GS0314 to K.K) and for Scientific Research (C) (20590426 to M.H) from Japanese Ministry of Education, Science, Culture, Sports, and Technology.

Appendix A. Supplementary data

Supplementary data associated with this article can be found, in the online version, at doi:10.1016/j.febslet.2009.03.071.

References

[1] Wilson, R.J.M. et al. (1996) Complete gene map of the plastid-like DNA of the malaria parasite *Plasmodium falciparum*. J. Mol. Biol. 261, 155–172.
[2] Ralph, S.A. et al. (2004) Tropical infectious diseases: metabolic maps and functions of the *Plasmodium falciparum* apicoplast. Nat. Rev. Microbiol. 2, 203–216.
[3] Dahl, E.L. and Rosenthal, P.J. (2008) Apicoplast translation, transcription and genome replication: targets for antimalarial antibiotics. Trends Parasitol. 24, 279–284.
[4] Sato, N., Terasawa, K., Miyajima, K. and Kabeya, Y. (2003) Organization, developmental dynamics, and evolution of plastid nucleoids. Int. Rev. Cytol. 232, 217–262.
[5] Swinger, K.K. and Rice, P.A. (2004) IHF and HU: flexible architects of bent DNA. Curr. Opin. Struct. Biol. 14, 28–35.
[6] Pettijohn, D.E. (1988) Histone-like proteins and bacterial chromosome structure. J. Biol. Chem. 263, 12793–12796.
[7] Bramhill, D. and Kornberg, A. (1988) A model for initiation at origins of DNA replication. Cell 54, 915–918.

[8] Aki, T. and Adhya, S. (1997) Repressor induced site-specific binding of HU for transcriptional regulation. EMBO J. 16, 3666–3674.
[9] Dri, A.M., Moreau, P.L. and Rouviere-Yaniv, J. (1992) Role of the histone-like proteins OsmZ and HU in homologous recombination. Gene 120, 11–16.
[10] Kobayashi, T., Takahara, M., Miyagishima, S.Y., Kuroiwa, H., Sasaki, N., Ohta, N., Matsuzaki, M. and Kuroiwa, T. (2002) Detection and localization of a chloroplast-encoded HU-like protein that organizes chloroplast nucleoids. Plant Cell 14, 1579–1589.
[11] Wu, H. and Liu, X.Q. (1997) DNA binding and bending by a chloroplast-encoded HU-like protein overexpressed in *Escherichia coli*. Plant Mol. Biol. 34, 339–343.
[12] Ram, E.V., Naik, R., Ganguli, M. and Habib, S. (2008) DNA organization by the apicoplast-targeted bacterial histone-like protein of *Plasmodium falciparum*. Nucleic Acids Res. 36, 5061–5073.
[13] Singh, D., Chaubey, S. and Habib, S. (2003) Replication of the *Plasmodium falciparum* apicoplast DNA initiates within the inverted repeat region. Mol. Biochem. Parasitol. 126, 9–14.
[14] Huisman, O., Faelen, M., Girard, D., Jaffe, A., Toussaint, A. and Rouviere-Yaniv, J. (1989) Multiple defects in *Escherichia coli* mutants lacking HU protein. J. Bacteriol. 171, 3704–3712.
[15] Dessens, J.T., Beetsma, A.L., Dimopoulos, G., Wengelnik, K., Crisanti, A., Kafatos, F.C. and Sinden, R.E. (1999) CTRP is essential for mosquito infection by malaria ookinetes. EMBO J. 18, 6221–6227.
[16] Hirai, M. et al. (2008) Male fertility of malaria parasites is determined by GCS1, a plant-type reproduction factor. Curr. Biol. 18, 607–613.
[17] Wada, M., Kano, Y., Ogawa, T., Okazaki, T. and Imamoto, F. (1988) Construction and characterization of the deletion mutant of *hupA* and *hupB* genes in *Escherichia coli*. J. Mol. Biol. 204, 581–591.
[18] Patankar, S., Munasinghe, A., Shoaibi, A., Cummings, L.M. and Wirth, D.F. (2001) Serial analysis of gene expression in *Plasmodium falciparum* reveals the global expression profile of erythrocytic stages and the presence of anti-sense transcripts in the malarial parasite. Mol. Biol. Cell 12, 3114–3125.
[19] Dri, A.M., Rouviere-Yaniv, J. and Moreau, P.L. (1991) Inhibition of cell division in *hupA hupB* mutant bacteria lacking HU protein. J. Bacteriol. 173, 2852–2863.
[20] Guo, L., Katayama, T., Seyama, Y., Sekimizu, K. and Miki, T. (1999) Isolation and characterization of novel cold-sensitive *dnaA* mutants of *Escherichia coli*. FEMS Microbiol. Lett. 176, 357–366.

THE JOURNAL OF BIOLOGICAL CHEMISTRY VOL. 284, NO. 46, pp. 31827–31833, November 13, 2009

Three Redox States of *Trypanosoma brucei* Alternative Oxidase Identified by Infrared Spectroscopy and Electrochemistry[S]

Received for publication, August 26, 2009, and in revised form, September 16, 2009 Published, JBC Papers in Press, September 19, 2009, DOI 10.1074/jbc.M109.059980

Amandine Maréchal[‡1], **Yasutoshi Kido**[§2], **Kiyoshi Kita**[§3], **Anthony L. Moore**[¶4], **and Peter R. Rich**[‡5]

From the [‡]*Glynn Laboratory of Bioenergetics, Institute of Structural and Molecular Biology, University College London, Gower Street, London WC1E 6BT, United Kingdom, the* [§]*Department of Biomedical Chemistry, Graduate School of Medicine, University of Tokyo, Hongo 7-3-1, Bunkyo-ku, Tokyo 113-0033, Japan, and the* [¶]*Department of Biochemistry and Biomedical Sciences, School of Life Sciences, University of Sussex, Falmer, Brighton BN1 9QG, United Kingdom*

Electrochemistry coupled with Fourier transform infrared (IR) spectroscopy was used to investigate the redox properties of recombinant alternative ubiquinol oxidase from *Trypanosoma brucei*, the organism responsible for African sleeping sickness. Stepwise reduction of the fully oxidized resting state of recombinant alternative ubiquinol oxidase revealed two distinct IR redox difference spectra. The first of these, signal 1, titrates in the reductive direction as an $n = 2$ Nernstian component with an apparent midpoint potential of 80 mV at pH 7.0. However, reoxidation of signal 1 in the same potential range under anaerobic conditions did not occur and only began with potentials in excess of 500 mV. Reoxidation by introduction of oxygen was also unsuccessful. Signal 1 contained clear features that can be assigned to protonation of at least one carboxylate group, further perturbations of carboxylic and histidine residues, bound ubiquinone, and a negative band at 1554 cm^{-1} that might arise from a radical in the fully oxidized protein. A second distinct IR redox difference spectrum, signal 2, appeared more slowly once signal 1 had been reduced. This component could be reoxidized with potentials above 100 mV. In addition, when both signals 1 and 2 were reduced, introduction of oxygen caused rapid oxidation of both components. These data are interpreted in terms of the possible active site structure and mechanism of oxygen reduction to water.

Mitochondria from many higher plants possess, in addition to the conventional cytochrome *c* oxidase, a second terminal oxidase that oxidizes ubiquinol (1–3). In thermogenic plants this alternative oxidase (AOX)[6] plays a key role in the release of heat for pollination purposes or for maintaining a warm environment within the flower at low ambient temperatures. In nonthermogenic plants its function is still under debate; proposed roles include maintaining tricarboxylic acid cycle turnover under high cytosolic phosphorylation potentials, defense against oxidative stress, and growth rate and energy charge homeostasis (4). AOX is also found in species of fungi, green algae, bacteria, and protozoa (5) and, more recently, in mollusks, nematodes, and chordates (6). Of particular importance, however, is its presence in pathogenic protozoa such as the blood parasite *Trypanosoma brucei* (7) and the intestinal parasite *Cryptosporidium parvum* (8, 9). *T. brucei* is a parasite that causes African sleeping sickness in humans and Nagana in livestock and is transmitted by the tsetse fly (7). The bloodstream forms of *T. brucei* appear to depend solely on its alternative oxidase (TAO) for respiration. Because the protein is absent from the mammalian host, TAO is an attractive and important chemotherapeutic target for African trypanosomiasis (7–10). In this respect it is interesting to note that ascofuranone, isolated from the pathogenic fungus *Ascochyta visiae*, specifically and potently inhibits the quinol oxidase activity of TAO (11) and rapidly kills the parasites. In addition, the chemotherapeutic efficacy of ascofuranone *in vivo* has been confirmed (12).

Compared with other respiratory chain complexes, the structure and mechanism of AOX are poorly characterized because of difficulties encountered in purification and a dearth of spectroscopic signatures. It has been proposed from sequence comparisons that AOX is a nonheme diiron carboxylate protein in which the metal atoms are ligated by glutamic acid and histidine residues within a four-helix bundle (1, 2, 13). The requirement for such a tertiary structural motif, as well as the necessary spacing between the iron-ligating amino acids, imposes considerable constraints upon overall possible three-dimensional structure and, consequently, its attachment to the membrane. The current model of the AOX, supported by mutagenesis studies, predicts a monotopic integral membrane protein (2, 13–15) associating with one leaflet of the lipid

[S] The on-line version of this article (available at http://www.jbc.org) contains supplemental Figs. S1–S3 and Table S1.

[1] Supported by a Wellcome Trust ViP award.
[2] Supported in part by Grant-in-aid for Young Scientists (B) 21790402.
[3] Supported by Creative Scientific Research Grant 18GS0314, Grant-in-aid for Scientific Research on Priority Areas 18073004 from the Japanese Society for the Promotion of Science, and a Targeted Proteins Research Program from the Japanese Ministry of Education, Science, Culture, Sports and Technology.
[4] Supported by the Biotechnology and Biological Sciences Research Council and the Prime Minister's Initiative 2 (Connect) fund for collaborative twinning with KK.
[5] Supported by Biotechnology and Biological Sciences Research Council Research Grant BB/H000097/1. To whom correspondence should be addressed. Tel.: 44-20-7679-7746; Fax: 44-20-7679-7096; E-mail: prr@ucl.ac.uk.

[6] The abbreviations used are: AOX, alternative oxidase; ATR, attenuated total reflection; δ_{IP}, in plane bending; FTIR, Fourier transform infrared; TAO, trypanosomal alternative oxidase; rTAO, recombinant TAO expressed in a heme-deficient strain of *E. coli*; ν_s and ν_{as}, symmetric and asymmetric stretching, respectively.

bilayer. Although analyses of yeast and trypanosomal enzymes have established that iron is required for activity (16, 17), early investigations of either mitochondria or partially purified protein failed to reveal spectroscopic signatures of its active site (18, 19). The first spectroscopic evidence for iron involvement was provided by Berthold *et al.* (20), who reported two EPR signals in *Escherichia coli* membranes that contained an overexpressed, truncated but active *Arabidopsis thaliana* alternative oxidase (AOX1a) fused to a maltose-binding protein. A signal around $g = 15$, observed with parallel mode EPR in reduced samples, was attributed to the diferrous state. A second signal, observed only after reaction of this state with oxygen, was assigned to a mixed valence ($Fe^{II}Fe^{III}$) form. More recently, Affourtit and Moore (21) prepared an active AOX protein from *Arum maculatum*. Parallel mode EPR studies (22) confirmed the presence of the diferrous signal in the reduced protein but attempts to generate the mixed valence signal of Berthold *et al.* (20) were not successful. Further spectroscopic tools are clearly desirable to resolve these inconsistencies, and, with this aim in mind, we report here the first electrochemical/FTIR study of a highly purified and stable preparation of recombinant AOX (rTAO) from *T. brucei*.

EXPERIMENTAL PROCEDURES

Isolation of rTAO—TAO was expressed in *E. coli* FN102 (Δ*hemA*) as described previously (23). In brief, rTAO was extracted by 1.4% (w/v) *n*-octyl-β-D-glucopyranoside, and, because rTAO was fused with an N-terminal histidine tag, solubilized rTAO was purified by cobalt affinity chromatography. The solubilized enzyme was bound to the cobalt affinity resin in the presence of detergent, and 100% of the rTAO activity was recovered from the column when *n*-octyl-β-D-glucopyranoside in the washing and elution buffers was exchanged with 0.042% (w/v) *n*-dodecyl-β-D-maltopyranoside. Finally, purified rTAO was obtained by two-step elution with 165 mM and 200 mM imidazole, which resulted in a very efficient purification of active rTAO in the presence of *n*-dodecyl-β-D-maltopyranoside (see supplemental Fig. S1). Specific activity of the final preparation was 207 μmol/min per mg using 150 μM ubiquinol-1.

ATR-FTIR Spectroscopy—Mid-IR spectra were recorded in ATR mode with a Bruker IFS/66S FTIR spectrophotometer fitted with a liquid nitrogen-cooled MCT-A detector at 4 cm^{-1} resolution, giving an accuracy of cited frequencies of ±1 cm^{-1}.

Sample Preparation—To remove the imidazole and to favor the interaction of the protein with the ATR prism surface, 100 μg of rTAO was diluted in 2.5 ml of 1 mM potassium phosphate buffer, pH/pD 7.0, and centrifuged at 450,000 × *g*, 4 °C, for 30 min. The pellet was resuspended with 2.5 ml of the same buffer and centrifuged for 15 min under the same conditions. The pellet was finally resuspended with 8 μl of 1 mM potassium phosphate, pH/pD 7.0. This solution was then quickly put on the ATR prism and dried under a nitrogen flow (4–5 min). The dried protein was rewetted with 10 μl of a 1 mM potassium phosphate buffer, pH/pD 7.0. The protein sample was stable with an amide II band intensity of 0.1–0.2.

Electrochemically Induced Spectroscopy—An ATR-FTIR-compatible cell with a platinum mesh working electrode was built on top of the sample layer. It was connected via a Vycor frit to a platinum sheet counter and Ag/AgCl reference electrodes (24). The chamber was filled with a freshly prepared mediator solution, and the sample was allowed to equilibrate for 1 h before starting any redox experiment. Buffer alone was placed in the reference/counter electrode chamber. All of the potential values are quoted relative to the normal hydrogen electrode.

Reduced minus oxidized spectra were induced electrochemically in 100 mM potassium phosphate, 100 mM KCl at pH/pD 7.0 and containing 500 μM potassium ferricyanide and 100 μM benzyl viologen as redox mediators. Working electrode potentials were +550 mV for oxidation and −400 mV for reduction. IR difference spectra were measured by recording a background spectrum (500 interferograms) at one potential, then switching to the second potential and recording a sample spectrum after a 13-min equilibration. Redox cycles were repeated 40 times in H_2O buffer (30 times in D_2O buffer), and reductive and oxidative spectra were averaged to produce the redox spectra shown.

For redox titration experiments, two different mixtures of mediators in 100 mM potassium phosphate, 100 mM KCl at pH 7.0 were tested: (i) 200 μM indigo trisulfonate ($n = 2$; $E_0' = -81$ mV) + 200 μM ruthenium hexamine ($n = 1$; $E_0' = +20$ mV) + 200 μM 2,4-naphthoquinone disulfonic acid ($n = 2$; $E_0' = +120$ mV) or (ii) 200 μM indigo trisulfonate + 200 μM 2,4-naphthoquinone disulfonic acid + 200 μM phenazine methosulfate ($n = 2$; $E_0' = +80$ mV) + 100 μM gallocyanine ($n = 2$; $E_0' = +20$ mV) + 1 mM ferricyanide ($n = 1$; $E_0' = +430$ mV). IR difference spectra were measured against a background spectrum of the fully oxidized (air-oxidized) sample. Reductive potentials between +200 mV and −100 mV were applied, and 15–20 min were required between two potential steps to achieve stability of the intensity of the two peak/troughs at 1658/1641 and 1544/1554 cm^{-1}. The signal amplitudes were expressed as a fraction of those of a reduced minus air-oxidized spectrum. They were plotted against potentials and simulated with the Nernstian equation,

$$y = \frac{1}{1 + \exp\left(\frac{(E_{1/2} - x) \times nF}{RT}\right)} \quad \text{(Eq. 1)}$$

where y is the oxidized fraction of TAO, x is the potential of the solution (in V), $E_{1/2}$ is the midpoint potential for the redox couple at pH 7.0, and n is the number of electrons involved in the reaction ($F = 96\,485$ C·mol^{-1}; $r = 8.314$ J·mol^{-1}·K^{-1}; $T = 298$ K). The reproducible data in Fig. 2 were obtained from a single 4-h titration.

Calculations of Vibrational Spectra—IR-active normal modes of tyrosine (Tyr-OH), tyrosinate (Tyr-O$^-$), and tyrosyl (Tyr-O$^\bullet$) were calculated on the UCL Legion parallel supercomputer cluster using Gaussian03 (25) with the B3LYP/6–13G(d) density functional and dataset. Data were obtained both for the zwitterionic free tyrosine as well as for tyrosine in a modified tripeptide (NH_2-Gly-Tyr-Gly-$COCH_3$) to better reflect protein environment. Molecular structures were first built with Facio (2006). Structures were then energy-minimized before calcu-

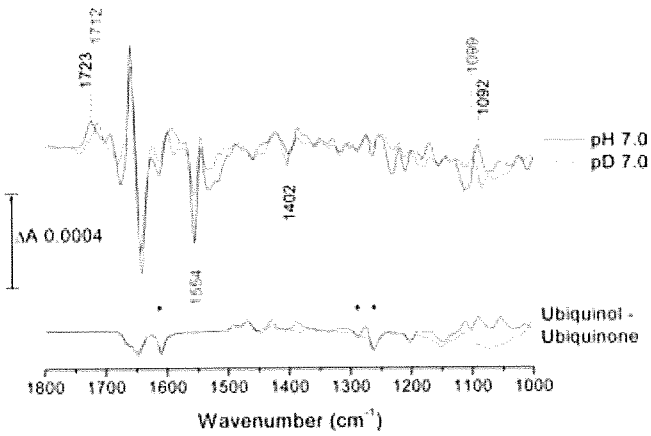

FIGURE 1. **Reduced minus oxidized IR difference spectrum of rTAO.** Reduction oxidation transformations were induced electrochemically in 100 mM potassium phosphate, 100 mM KCl at pH (*black trace*)/pD (*red trace*) 7.0 and containing 500 μM potassium ferricyanide and 100 μM benzyl viologen as redox mediators. Working electrode potentials were −400 mV for reduction and +550 mV for oxidation. For further details, see "Experimental Procedures." Published ubiquinol-10 minus ubiquinone-10 redox spectra recorded in both H_2O (*black*) and D_2O (*red*) media are also displayed for qualitative comparisons (37).

lating frequencies. Frequencies cited have been multiplied by the published scaling factor of 0.9614 (25).

RESULTS AND DISCUSSION

Secondary Structure Estimation—Information on protein secondary structure can be obtained from analyses of component bands within the amide I envelope of absolute IR absorption spectra (26, 27). Such an analysis performed on the IR spectra of rTAO in both H_2O and D_2O media predicts a minimum of 30% α-helix content in the rTAO secondary structure and up to 64% if rTAO can adopt a coiled-coil arrangement (see supplemental Table S1) (28, 29), as would occur if rTAO is folded to form the predicted four-helix bundle.

Reduced Minus Oxidized FTIR Difference Spectra—IR redox difference spectra of TAO obtained by electrochemistry at pH/pD 7.0 are shown in Fig. 1. The data were recorded in both H_2O (black) and D_2O (red) media to aid assignments. As with most redox proteins, the largest IR bands are found in the amide I (peak/trough at 1658/1641 cm^{-1}) and amide II (peak/trough at 1544/1554 cm^{-1}) regions and most commonly arise from changes in the amide I (predominantly C=O) and amide II (predominantly N–H) bands of the polypeptide backbone amide linkages. The assignment of the 1658/1641 cm^{-1} bands to redox-dependent amide I changes is strengthened by their very weak sensitivity to H/D exchange. In contrast, amide II bands are strongly shifted (≈−100 cm^{-1}) by H/D exchange, which is not the case for the 1554/1544 cm^{-1} bands. An estimation of the extent of H/D exchange from absolute IR absorption spectrum of rTAO recorded in D_2O *versus* H_2O (30) indicated that it was more than 95%. Hence, it is unlikely that the lack of shift was caused by poor H/D exchange, and other possible origins of the trough/peak at 1554/1544 cm^{-1} are discussed below.

An informative feature in the redox spectra is the positive peak at 1723 cm^{-1} in H_2O that is downshifted to 1712 cm^{-1} on H/D exchange. Bands in this frequency range with such H/D shifts are generally characteristic of protonated carboxyl groups (31, 32). There is no associated trough of equal magnitude in this region, ruling out the possibility that the carboxyl group(s) is also protonated in the oxidized state. However, a trough of roughly equal intensity was observed at 1402 cm^{-1}, slightly up-shifted (+2 cm^{-1}) on H/D exchange, together with a broad trough that underlies sharper bands in the 1560–1500 cm^{-1} amide II region. Taken together, these bands suggest the loss on reduction of the ν_s and ν_{as} vibrational modes of a deprotonated carboxylate group at 1402 and ~1530 cm^{-1} that is linked with the appearance of the 1723 cm^{-1} C=O peak of its protonated form. Hence, we conclude that reduction of rTAO results in the net protonation of one or more carboxylate groups. Deconvolution of both the H_2O and D_2O spectra with multiple Gaussian functions in the 1750-1700 cm^{-1} region (see supplemental Fig. S2) suggests that more than one carboxyl group may contribute. The best fit was obtained with two carboxyl groups being protonated (peaks at 1725 and 1717 cm^{-1} in H_2O, 1715 and 1709 cm^{-1} in D_2O) and one protonated carboxyl group changing conformation/environment on reduction (trough/peak at 1749/1735 cm^{-1} in H_2O, shifted by −8 cm^{-1} and more evident in the D_2O spectrum).

Other features around 1100 cm^{-1} are likely to arise from histidine changes (31, 33). In particular, the intense peak at 1092 cm^{-1}, upshifted to 1099 cm^{-1} in D_2O, is consistent with perturbation of an Nτ-protonated histidine bound by its Nπ to a metal center (34), as is found in the active sites of other homologous diiron proteins (35).

Finally, because reduced ubiquinone-9 is known to be the TAO electron donor in the bloodstream form of the trypanosome (36), we compared the rTAO redox spectra with published ubiquinone redox spectra recorded in both H_2O and D_2O media (37). Several bands are evident that correspond to those seen in the reference ubiquinone spectra (Fig. 1), particularly the bands at 1263 and 1289 cm^{-1} (arising from methoxy/quinone ring modes) and at 1612 cm^{-1} (from quinone C=C bonds) (38).

Redox Titration—The presence of an FTIR redox signature in rTAO provided a means to determine the redox properties of its active site by controlled potentiometry in a combined electrochemical/ATR-FTIR device (24). Redox mediators were chosen to cover the potential range from +200 to −100 mV (see "Experimental Procedures"). Fig. 2*A* presents the spectra recorded during the first reductive titration of a freshly prepared protein layer in 100 mM potassium phosphate, 100 mM KCl, at pH 7.0. The extent of reduction was estimated from the magnitudes of the two peak/troughs at 1658/1641 and 1544/1554 cm^{-1} and, typically, 15–20 min were required between two potential steps to allow their stabilization. The extent of reduction is plotted against ambient potential in Fig. 2*B*. It displayed the Nernstian behavior expected for an $n = 2$ reduction with a midpoint potential of +80 mV at pH 7.0 (see overlays in Fig. 2*B*). However, attempts to reverse the titration without hysteresis in the oxidative direction were unsuccessful, and no reoxidation was observable until potentials above +500 mV were applied (see below). Hence, it is not possible to conclude that the behavior seen in the reductive direction represents the equilibrium thermodynamic properties of this redox transition.

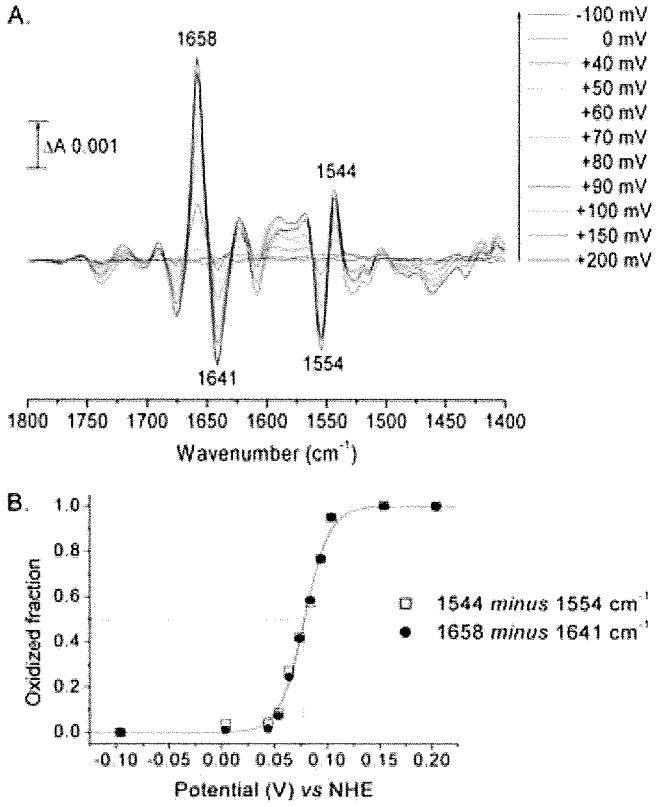

FIGURE 2. **Reductive titration of rTAO.** *A*, difference spectra recorded during a reductive titration in 100 mM potassium phosphate, 100 mM KCl at pH 7.0 (see "Experimental Procedures"). *B*, plots of peak/trough intensities at 1658/1641 and 1544/1554 cm^{-1} *versus* potential. Data were simulated with a Nernst-derived equation for an $n = 2$ component with $E_{1/2} = 79$ mV.

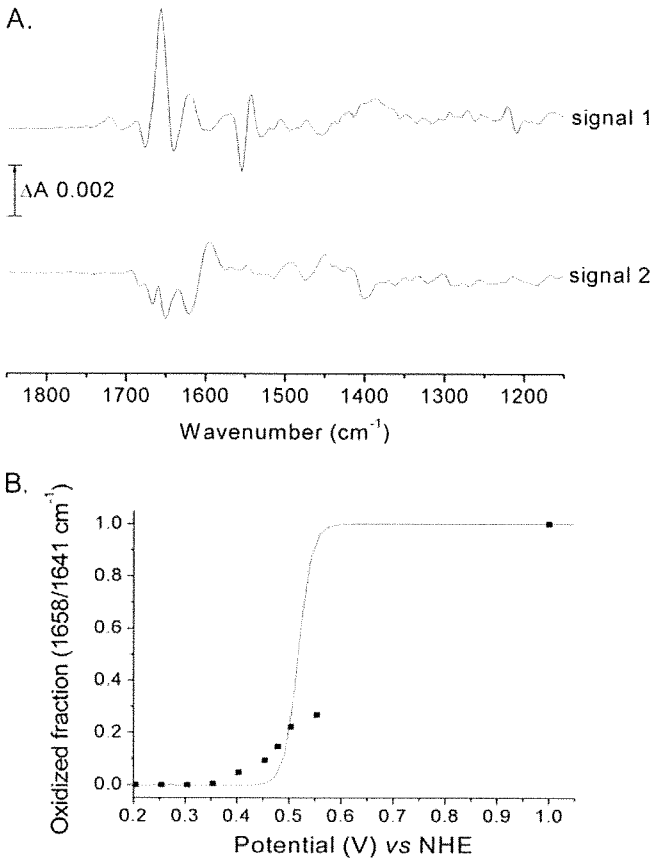

FIGURE 3. **Separation of redox spectra and oxidative titration of signal 1.** *A*, a fully oxidized spectrum was recorded and use as a background. Potential was set to −10 mV, and signal 1 was recorded after 20 min. A new background spectrum was then recorded, and signal 2 was observed to develop at 1 h. *B*, oxidative titration of signal 1 at pH 7.0 with a mixture of redox mediators containing ferricyanide. Data were simulated with a Nernst-derived equation (see "Experimental Procedures") for an $n = 2$ component with $E_{1/2} = 520$ mV (*solid line*) or for an unrestricted fit which gave $n = 0.6$ and $E_{1/2} = 510 \pm 30$ mV (*dotted line*). The maximum intensity of signal 1 was determined by the addition of dioxygen to the fully reduced state.

Introduction of oxygen into the sample when this component had become reduced also failed to promote reoxidation, indicating that this reduced state is not the oxygen-reactive species.

Further investigations revealed that there was a second redox component that was becoming reduced much more slowly than the redox component represented by the two peak/troughs at 1658/1641 and 1544/1554 cm^{-1} and termed "signal 1." This could be detected most clearly after reduction of a fully oxidized sample for 20 min at −10 mV, at which time signal 1 was fully developed and the second component remained mostly oxidized (Fig. 3*A*, *signal 1*). Maintenance of the ambient potential at −10 mV led to the appearance of a second distinct redox IR spectrum that we have termed "signal 2." Its reduction was slow (1 h at −10 mV) but, in contrast to signal 1, could be reoxidized slowly by moderate oxidizing potentials (1 h at +200 mV). A full titration of this second redox couple could not be achieved because of overlap with signal 1 and its very slow rate of redox equilibration. Nevertheless, by prereduction of both signals 1 and 2, followed by reoxidation of signal 2, a reduced minus oxidized spectrum of signal 2 alone could be obtained (Fig. 3*A*, *signal 2*), and an approximate midpoint potential around +50 mV could be estimated. Signals 1 and 2 are quite distinct components. For example, there is no signature of protonated carboxyl group at 1723 cm^{-1} or evidence of bands at 1544/1554 cm^{-1} in signal 2. These spectra are not shown below 1200 cm^{-1} because the redox mediators used also absorb in this region, and no corrections for their contributions were made.

After full reduction of both signals 1 and 2, the fully oxidized starting state of rTAO could be regenerated within the time scale of recording by introduction of O_2 into the electrochemistry cell. This contrasts markedly with the oxygen-insensitive behavior observed when only signal 1 was reduced. After reoxidation with molecular oxygen when signals 1 and 2 were reduced, signals 1 and 2 could then be titrated as before. These observations show that both redox components must be reduced to produce a form that can react with oxygen to regenerate the fully oxidized state.

In an attempt to titrate signal 1 oxidatively, redox titrations were performed with a mixture of mediators containing ferricyanide to allow equilibration at higher potentials (see "Experimental Procedures"). After full reduction of signals 1 and 2 (approximately 1.5 h at −10 mV) and oxidation of signal 2 only (approximately 1 h at +200 mV), potentials were stepped to higher values (see Fig. 3*B*). After 2.5 h with potentials as high as +550 mV, only a fraction (≈25%) of signal 1 was oxidized. We verified this was not due to protein instability by reduction back to the fully reduced form of rTAO and reintroduction of O_2, thereby regenerating 100% of the fully oxidized state. These

observations suggest that potentials in excess of +550 mV are required for full signal 1 reoxidation, which is beyond the limit of accessible electrochemistry with the platinum grid/ferricyanide system. This behavior explains the low signal amplitudes of the rTAO data of Fig. 1 because the data are an average of cyclical reductions and oxidations without introduction of oxygen to regenerate the oxidized state fully and without a very long time at reducing potentials to reduce signal 2 fully. The cycle of reduction of signal 1 and signal 2 followed by injection of O_2 into the electrochemistry cell to restore the fully oxidized resting state could be repeated reproducibly over many cycles, indicating that the enzyme itself remained very stable during the course of these investigations.

By comparison of band intensities at 1263 and 1612 cm^{-1} of a full redox spectrum of an optimized protein layer with those of a standardized solution of ubiquinone-10 in chloroform (see supplemental Fig. S3), a ubiquinone concentration in the layer was estimated to be approximately 4 mM. Previously, it has been shown that a layer of bovine cytochrome *c* oxidase (molecular mass, 204,000 Da; amide II band, approximately 0.25 ΔA) is maximally 1.8 mM (based on perfect packing) (39). Hence, the rTAO concentration (molecular mass, 34,000 Da; amide II band, 0.22 ΔA) could be up to 9 mM. As a result, it is concluded that the rTAO has retained ubiquinone such that its Q site is partially occupied with substrate ubiquinone.

Relevance to Catalytic Cycle—This study has revealed two redox processes that have distinct IR signatures, signal 1 and signal 2. Signal 1 could be titrated in the reductive direction where it behaved as if it were an $n = 2$ process with a midpoint potential of +80 mV at pH 7.0. However, the reaction was not reversible over the same potential range, indicating that this does not represent its equilibrium thermodynamic properties, a conclusion confirmed by the observation that even partial reoxidation of signal 1 could be achieved only with potentials of +550 mV. Such behavior can be observed in $n = 2$ redox systems when the one-electron intermediate is highly unstable, such as is seen, for example, in cyclic voltammetric behavior of quinones (40). In this case, reduction is controlled by the low potential reduction of quinone to semiquinone, whereas quinol oxidation is controlled by the high potential step of quinol oxidation to semiquinone. Hence, both oxidative and reductive waves appear only at overpotentials compared with the equilibrium $n = 2$ potential. It is possible that the behavior of signal 1 arises from a similar phenomenon in which it is an $n = 2$ reaction, but with a highly unstable one-electron form. In this case, the true thermodynamic $n = 2$ midpoint potential will lie somewhere between the observable reductive and oxidative waves. It is also possible that reduction of signal 1 by mediators is indirect, being mediated by the ubiquinone that is bound to the protein and that it is the known redox hysteresis of the ubiquinone that gives rise to the signal 1 behavior. A further possibility is that reduction of signal 1 induces a conformational change of the protein, raising the signal 1 potential to much higher values, a type of behavior that has been proposed to explain hysteresis of cytochrome cd_1 redox titrations (41).

Signal 2 behaves more conventionally in that it appears to be reversibly oxidized and reduced over the same potential range, with a midpoint potential around +50 mV. However, its equilibration was far too slow to be able to perform an accurate redox titration to determine whether it had an *n* value of 1 or 2. These slow kinetics are not limited by diffusion of mediators between electrode and protein layer. They most likely arise because of slow equilibration between mediators and the redox group(s) involved.

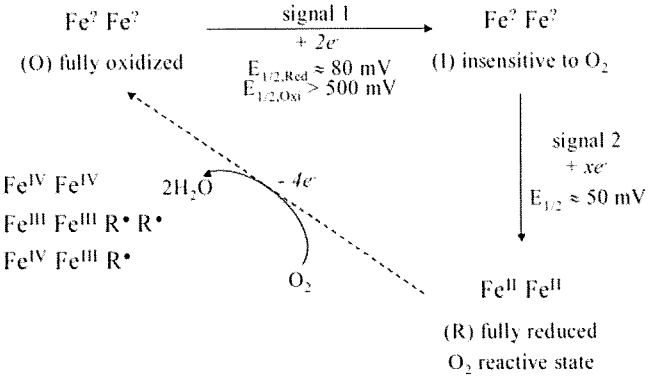

FIGURE 4. **Summary of experimental observations and their relation to the catalytic cycle of reduction of oxygen to water.**

In Fig. 4, a working model is proposed of the relationship between these IR-observed species and the physiological reaction cycle of the 4-electron reduction of dioxygen to water. Starting from the fully oxidized resting state of TAO (O), a 2-electron reduction occurs, represented by signal 1. This produces a species (I) that is insensitive to the presence of dioxygen. The (I) minus (O) IR difference spectrum shows clearly the net protonation of at least one carboxylate residue, and this is likely to give the transition a pH-dependent midpoint potential. In addition, the complexity of the carboxylic acid region changes, indicative of an additional underlying carboxylic acid shift, together with perturbations in the 1100 cm^{-1} region that indicate histidine alterations, are consistent with the proposed involvement of glutamic and histidine residues in the active site (1, 2, 13).

Species (I) can be further reduced, most probably with two electrons, to give a third redox state (R) that is the oxygen-reactive form. (R) must presumably correspond to the diferrous state that gives rise to the spin-coupled $Fe^{II}Fe^{II}$ EPR signal at $g \geq 15$ that was observed in dithionite-reduced samples by Berthold *et al.* (20) and Moore *et al.* (22). The need to reduce TAO fully to react with oxygen to form the (O) state might be related to the observation of Berthold *et al.* that an $Fe^{II}Fe^{III}$ mixed-valence state could only be observed by oxidation of the fully reduced state with oxygen (42). However, because of the differences in protocol details, it is not possible at present to determine whether the mixed-valence form should correspond to (O) or (I).

(R) can react rapidly with dioxygen to regenerate the fully oxidized (O) state. Because 4 electrons are required for reduction of dioxygen to water, the oxidation state of (O) will depend on whether the electrons are provided solely by the two metals, by protein residue(s) that produce radicals, or by substrate ubiquinol. Hence, if the (O) state does indeed result in formation of water, it must be (i) a diferryl center ($Fe^{IV}Fe^{IV}$); (ii) a diferric center plus two radicals ($Fe^{III}Fe^{III}R^{\bullet}R^{\bullet}$); (iii) a mixed-

valence ferryl/ferric center plus a radical ($Fe^{IV}Fe^{III}R^{\bullet}$) (3). All of these species are potentially EPR-silent. Such radicals could arise from amino acids or, possibly, substrate ubiquinol. Reduction of (O) to (I) most likely involves addition of two reducing equivalents into the (O) state that reduce the metals and/or radicals. Finally, it also remains possible that oxygen is incompletely reduced in the (O) state, which could, for example, contain a bound peroxide that becomes reduced in the (O) to (I) transition. Such a species could well explain the irreversibility of the reduction. However, it is difficult to reconcile a peroxide species with the formation of a mixed-valence form, and so this possibility presently seems unlikely.

In the R2 subunit of the ribonucleotide reductase, a well characterized diiron carboxylate protein, a tyrosyl residue is involved in catalysis. The fact that this residue is buried deeply into the protein structure provides it with a peculiar stability (up to several days) (43). Mutagenesis studies of both the plant AOX (44) and TAO (15) have revealed that tyrosine 275 is crucial for catalysis. This tyrosine or, possibly, a nearby tryptophan 206 (*Sauromatum guttatum* numbering) might provide a radical site (44, 45); hence a role for radical(s) in the TAO catalytic cycle seems likely. The sharp H/D-insensitive negative band at 1554 cm^{-1} could arise from the loss of a radical in the (O) to (I) transformation. Radicals of ubiquinone are expected to have a sharp band around 1490 cm^{-1}. IR and Raman features of neutral phenoxyl radical models and tyrosine radicals in proteins show two prominent modes of the neutral phenolic radical identified as ν_{8a}(C–C) at 1550–1610 cm^{-1} and ν_{7a}(C–O) at 1480–1530 cm^{-1}, and the radical state of TyrD in photosystem II shows two bands at 1551 and 1503 cm^{-1} (46–48). Moreover, density functional theory simulations (see "Experimental Procedures") of a neutral tyrosyl radical in both free zwitterionic tyrosine and in a model peptide also predict a strong band at 1554 cm^{-1}. In contrast, the rather limited IR data on tryptophanyl radicals indicate that they have IR bands at higher frequencies (49). Hence, if the 1554 cm^{-1} band does indeed arise from a radical, a tyrosyl species in the (O) state is currently most favored. Ground-state tyrosine in its protonated form is known to have bands at 1508 cm^{-1} and, in the tyrosinate form, at 1547 cm^{-1}. These bands also appear in density functional theory simulations, with an assignment to a normal mode arising from ν(C–O) + ν_s(C–C_{ring}) + δ_{IP}(H–C_{ring}). Hence, if the 1544/1554 cm^{-1} peak/trough in signal 1 does arise from tyrosine, then it most closely resembles the loss of a neutral tyrosyl radical in (O) and formation of a tyrosinate in (I) and (R). In any case, such a stable tyrosyl radical would have to be in an unusual environment in TAO, and stabilization of the tyrosinate state in (I) should make the formation of a radical energetically more facile. Further IR work on TAO and related diiron proteins, in particular a combination of FTIR and EPR analyses of the same redox states, should resolve both the nature of the mixed valence form and the involvement and types of any radicals.

REFERENCES

1. Finnegan, P. M., Soole, K. L., and Umbach, A. L. (2004) *Plant Mitochondria: From Genome To Function*, p. 163, Kluwer Academic Publishers, Dordrecht, The Netherlands
2. Berthold, D. A., and Stenmark, P. (2003) *Annu. Rev. Plant. Biol.* **54,** 497–517
3. Affourtit, C., Albury, M. S., Crichton, P. G., and Moore, A. L. (2002) *FEBS Lett.* **510,** 121–126
4. Moore, A. L., Albury, M. S., Crichton, P. G., and Affourtit, C. (2002) *Trends Plant Sci.* **7,** 478–481
5. McDonald, A. E., and Vanlerberghe, G. C. (2006) *Comp. Biochem. Physiol. D* **1,** 357–364
6. McDonald, A., and Vanlerberghe, G. (2004) *IUBMB Life* **56,** 333–341
7. Chaudhuri, M., Ott, R. D., and Hill, G. C. (2006) *Trends Parasitol.* **22,** 484–491
8. Roberts, C. W., Roberts, F., Henriquez, F. L., Akiyoshi, D., Samuel, B. U., Richards, T. A., Milhous, W., Kyle, D., McIntosh, L., Hill, G. C., Chaudhuri, M., Tzipori, S., and McLeod, R. (2004) *Int. J. Parasitol.* **34,** 297–308
9. Suzuki, T., Hashimoto, T., Yabu, Y., Kido, Y., Sakamoto, K., Nihei, C., Hato, M., Suzuki, S., Amano, Y., Nagai, K., Hosokawa, T., Minagawa, N., Ohta, N., and Kita, K. (2004) *Biochem. Biophys. Res. Commun.* **313,** 1044–1052
10. Nihei, C., Fukai, Y., and Kita, K. (2002) *Biochim. Biophys. Acta* **1587,** 234–239
11. Minagawa, N., Yabu, Y., Kita, K., Nagai, K., Ohta, N., Meguro, K., Sakajo, S., and Yoshimoto, A. (1997) *Mol. Biochem. Parasitol.* **84,** 271–280
12. Yabu, Y., Yoshida, A., Suzuki, T., Nihei, C., Kawai, K., Minagawa, N., Hosokawa, T., Nagai, K., Kita, K., and Ohta, N. (2003) *Parasitol. Int.* **52,** 155–164
13. Andersson, M. E., and Nordlund, P. (1999) *FEBS Lett.* **449,** 17–22
14. Berthold, D. A., Andersson, M. E., and Nordlund, P. (2000) *Biochim. Biophys. Acta* **1460,** 241–254
15. Nakamura, K., Sakamoto, K., Kido, Y., Fujimoto, Y., Suzuki, T., Suzuki, M., Yabu, Y., Ohta, N., Tsuda, A., Onuma, M., and Kita, K. (2005) *Biochem. Biophys. Res. Commun.* **334,** 593–600
16. Minagawa, N., Sakajo, S., Komiyama, T., and Yoshimoto, A. (1990) *FEBS Lett.* **267,** 114–116
17. Ajayi, W. U., Chaudhuri, M., and Hill, G. C. (2002) *J. Biol. Chem.* **277,** 8187–8193
18. Rich, P. R. (1978) *FEBS Lett.* **96,** 252–256
19. Berthold, D. A., and Siedow, J. N. (1993) *Plant Physiol.* **101,** 113–119
20. Berthold, D. A., Voevodskaya, N., Stenmark, P., Gräslund, A., and Nordlund, P. (2002) *J. Biol. Chem.* **277,** 43608–43614
21. Affourtit, C., and Moore, A. L. (2004) *Biochim. Biophys. Acta* **1608,** 181–189
22. Moore, A. L., Carré, J. E., Affourtit, C., Albury, M. S., Crichton, P. G., Kita, K., and Heathcote, P. (2008) *Biochim. Biophys. Acta* **1777,** 327–330
23. Nihei, C., Fukai, Y., Kawai, K., Osanai, A., Yabu, Y., Suzuki, T., Ohta, N., Minagawa, N., Nagai, K., and Kita, K. (2003) *FEBS Lett.* **538,** 35–40
24. Rich, P. R., and Iwaki, M. (2007) *Mol. BioSys.* **3,** 398–407
25. Frisch, M. J., Trucks, G. W., Schlegel, H. B., Scuseria, G. E., Robb, M. A., Cheeseman, J. R., Montgomery, J. A., Jr., Vreven, T., Kudin, K. N., Burant, J. C., Millam, J. M., Iyengar, I. I., Tomasi, J., Barone, V., Mennucci, B., Cossi, M., Scalmani, G., Rega, N., Petersson, G. A., Nakasuji, H., Hada, M., Ehara, M., Toyota, K., Fukuda, R., Hasegawa, J., Ishida, M., Nakajima, T., Honda, Y., Kitao, O., Nakai, H., Klene, M., Li, X., Knox, J. E., Hratchian, H. P., Cross, J. B., Bakken, V., Adamo, C., Jaramillo, J., Gomperts, R., Stratmann, R. E., Yazyev, O., Austin, A. J., Cammi, R., Pomelli, C., Ochterski, J. W., Ayala, P. Y., Morokuma, K., Voth, G. A., Salvador, P., Dannenberg, J. J., Zakrzewski, G., Dapprich, S., Daniels, A. D., Strain, M. C., Farkas, O., Malick, D. K., Rabuck, A. D., Raghavachari, K., Foresman, J. B., Ortiz, J. V., Cui, Q., Baboul, A. G., Clifford, S., Cioslowski, J., Stefanov, B. B., Liu, G., Liashenko, A., Piskorz, P., Komaromi, I., Martin, R. L., Fox, D. J., Keith, T., Al-Laham, M. A., Peng, C. Y., Nanayakkara, A., Challacombe, M., Gill, P. M. W., Johnson, B., Chen, W., Wong, M. W., Gonzalez, C., and Pople, J. A. (2005) *Gaussian 03*, Gaussian, Inc., Wallingford, CT
26. Arrondo, J. L. R., Muga, A., Castresana, J., and Goñi, F. M. (1993) *Prog. Biophys. Mol. Biol.* **59,** 23–56
27. Arrondo, J. L. R., and Goñi, F. M. (1999) *Prog. Biophys. Mol. Biol.* **72,** 367–405
28. Heimburg, T., Schuenemann, J., Weber, K., and Geisler, N. (1996) *Biochemistry* **35,** 1375–1382
29. Reisdorf, W. C., Jr., and Krimm, S. (1996) *Biochemistry* **35,** 1383–1386

30. Glasoe, P. K., and Long, F. A. (1960) *J. Phys. Chem.* **64,** 188–190
31. Barth, A. (2000) *Prog. Biophys Mol. Biol.* **74,** 141–173
32. Rich, P. R., and Iwaki, M. (2005) *Biophysical and Structural Aspects of Bioenergetics*, p. 314, The Royal Society of Chemistry, Cambridge, UK
33. Iwaki, M., Yakovlev, G., Hirst, J., Osyczka, A., Dutton, P. L., Marshall, D., and Rich, P. R. (2005) *Biochemistry* **44,** 4230–4237
34. Noguchi, T., Inoue, Y., and Tang, X.-S. (1999) *Biochemistry* **38,** 10187–10195
35. Solomon, E. I., Brunold, T. C., Davis, M. I., Kemsley, J. N., Lee, S.-K., Lehnert, N., Neese, F., Skulan, A. J., Yang, Y.-S., and Zhou, J. (2000) *Chem. Rev.* **100,** 235–350
36. Clarkson, A. B., Jr., Bienen, E. J., Pollakis, G., and Grady, R. W. (1989) *J. Biol. Chem.* **264,** 17770–17776
37. Iwaki, M., Giotta, L., Akinsiku, A. O., Schägger, H., Fisher, N., Breton, J., and Rich, P. R. (2003) *Biochemistry* **42,** 11109–11119
38. Breton, J., and Nabedryk, E. (1996) *Biochim. Biophys. Acta* **1275,** 84–90
39. Iwaki, M., and Rich, P. R. (2004) *J. Am. Chem. Soc.* **126,** 2386–2389
40. Rich, P. R. (2004) *Biochim. Biophys. Acta* **1658,** 165–171
41. Koppenhöfer, A., Turner, K. L., Allen, J. W. A., Chapman, S. K., and Ferguson, S. J. (2000) *Biochemistry* **39,** 4243–4249
42. Voevodskaya, N., Narvaez, A.-J., Domkin, V., Torrents, E., Thelander, L., and Gräslund, A. (2006) *Proc. Natl. Acad. Sci. U.S.A.* **103,** 9850–9854
43. Atkin, C. L., Thelander, L., Reichard, P., and Lang, G. (1973) *J. Biol. Chem.* **248,** 7464–7472
44. Albury, M. S., Affourtit, C., Crichton, P. G., and Moore, A. L. (2002) *J. Biol. Chem.* **277,** 1190–1194
45. Moore, A. L., and Albury, M. S. (2008) *Biochem. Soc. Trans.* **36,** 1022–1026
46. Berthomieu, C., and Hienerwadel, R. (2005) *Biochim. Biophys. Acta* **1707,** 51–66
47. Berthomieu, C., Boullais, C., Neumann, J.-M., and Boussac, A. (1998) *Biochim. Biophys. Acta* **1365,** 112–116
48. Berthomieu, C., Hienerwadel, R., Boussac, A., Breton, J., and Diner, B. A. (1998) *Biochemistry* **37,** 10547–10554
49. Walden, S. E., and Wheeler, R. A. (1996) *J. Chem. Soc. Perkin Trans.* **2,** 2663–2672

Acta Crystallographica Section F
Structural Biology and Crystallization Communications
ISSN 1744-3091

Overproduction, purification, crystallization and preliminary X-ray diffraction analysis of *Trypanosoma brucei gambiense* glycerol kinase

Emmanuel Oluwadare Balogun,[a,b] Daniel Ken Inaoka,[a] Yasutoshi Kido,[a] Tomoo Shiba,[a] Takeshi Nara,[c] Takashi Aoki,[c] Teruki Honma,[d] Akiko Tanaka,[d] Masayuki Inoue,[e] Shigeru Matsuoka,[e] Paul A. M. Michels,[f] Shigeharu Harada[g]* and Kiyoshi Kita[a]*

[a]Department of Biomedical Chemistry, Graduate School of Medicine, The University of Tokyo, 7-3-1 Hongo, Bunkyo-ku, Tokyo 113-0033, Japan, [b]Department of Biochemistry, Ahmadu Bello University, Zaria, Nigeria, [c]Department of Molecular and Cellular Parasitology, Juntendo University School of Medicine, Tokyo 113-8421, Japan, [d]Systems and Structural Biology Center, RIKEN, Tsurumi, Yokohama 230-0045, Japan, [e]Graduate School of Pharmaceutical Sciences, The University of Tokyo, Tokyo 113-0033, Japan, [f]Research Unit for Tropical Diseases, de Duve Institute and Laboratory of Biochemistry, Université Catholique de Louvain, Avenue Hippocrate 74, B-1200 Brussels, Belgium, and [g]Department of Applied Biology, Graduate School of Science and Technology, Kyoto Institute of Technology, Sakyo-ku, Kyoto 606-8585, Japan

Correspondence e-mail: harada@kit.ac.jp, kitak@m.u-tokyo.ac.jp

Received 7 September 2009
Accepted 5 January 2010

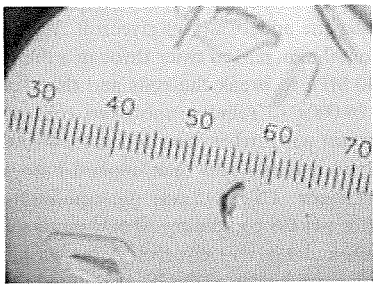

In the bloodstream forms of human trypanosomes, glycerol kinase (GK; EC 2.7.1.30) is one of the nine glycosomally compartmentalized enzymes that are essential for energy metabolism. In this study, a recombinant *Trypanosoma brucei gambiense* GK (rTbgGK) with an N-terminal cleavable His_6 tag was overexpressed, purified to homogeneity and crystallized by the sitting-drop vapour-diffusion method using PEG 400 as a precipitant. A complete X-ray diffraction data set to 2.75 Å resolution indicated that the crystals belonged to the orthorhombic space group $P2_12_12_1$, with unit-cell parameters a = 63.84, b = 121.50, c = 154.59 Å. The presence of two rTbgGK molecules in the asymmetric unit gives a Matthews coefficient (V_M) of 2.5 $Å^3$ Da^{-1}, corresponding to 50% solvent content.

1. Introduction

Human African trypanosomiasis (HAT) is a neglected haemoparasitic disease caused by species of the protozoan genus *Trypanosoma* and transmitted by tsetse flies. Over 20 000 new cases are reported annually; it is also a threat to 60 million human lives (World Health Organization, 2006). The human pathogens for the disease are *T. brucei gambiense* and *T. b. rhodesiense*, which cause West and East African trypanosomiasis, respectively, with animals serving as their reservoirs (Njiokou *et al.*, 2006), while the animal pathogens include *T. b. brucei*, *T. vivax*, *T. congolense* and *T. evansi* (Stevens & Brisse, 2004). HAT occurs in two forms: an acute form caused by *T. b. rhodesiense* and a chronic form caused by *T. b. gambiense*. Both agents of the disease present an early haemolymphatic stage and a late meningoencephalitic phase and are deadly at the second stage if left untreated. Unfortunately, only a few drugs are available and problems such as narrow spectrum, treatment failures owing to resistance, high cost and cases of toxicity have been reported (Brun *et al.*, 2001). Therefore, the need to search for new, safer, affordable and more effective drugs with a broader spectrum of action cannot be overemphasized.

Interestingly, the bloodstream forms (BSFs) of these parasites possess several structural and metabolic features that are absent in the mammalian hosts. Such distinctive features, which provide valid drug targets, include compartmentalization of their glycolysis into microbody-like organelles called glycosomes, their sole dependence on glycolysis for their energy needs (Haanstra *et al.*, 2008) and the presence of a rudimentary mitochondrion that houses an indispensable cytochrome-independent alternative oxidase (AOX; Chaudhuri *et al.*, 2006). AOX is not found in the host and its inhibition by salicylhydroxamic acid (SHAM) or ascofuranone (AF) has been reported to cause parasite death as a result of impaired ATP metabolism (Minagawa *et al.*, 1997; Michels *et al.*, 2000; Hannaert *et al.*, 2003; Guerra *et al.*, 2006; Yabu *et al.*, 2006; Singha *et al.*, 2008). In addition, trypanosomes contain a unique glycerol kinase (GK) in their glycosomes. Unlike the host GK, which only catalyses the forward reaction, *i.e.* ATP-dependent glycerol phosphorylation, trypanosomal GK can also catalyze the reverse reaction (Kralova *et al.*, 2000).

Our laboratory has found AF to be an excellent inhibitor of trypanosomal AOX (TAO): its K_i against TAO is 2.38 n*M* (Minagawa *et al.*, 1997) compared with 10 μ*M* for the previously discovered TAO inhibitor SHAM (Njogu *et al.*, 1980). However, *in vitro* and *in vivo* experiments have revealed that AF-induced or SHAM-induced killing of trypanosomes is considerably enhanced when they are co-administered with 5 m*M* glycerol (Fairlamb *et al.*, 1977; Van der Meer & Versluijs-Broers, 1979; Minagawa *et al.*, 1997; Yabu *et al.*, 2006). This synergistic effect of glycerol is most likely to be mediated *via* an expected mass-action-induced inhibition of GK by the added glycerol, thereby blocking the anaerobic ATP generation of glycolysis in the parasites. Unfortunately, this nonphysiologically high concentration of glycerol required for co-administration with AF is toxic to the host. Although GK in conjunction with TAO is thus a promising target for chemotherapy, an effective and selective parasite GK inhibitor has not yet become available.

GK is ubiquitous in archaea, bacteria and eukaryotes, where it belongs to the sugar kinase/heat-shock protein 70/actin superfamily (Hurley, 1996). To date, prokaryotic GKs have been the most widely studied. Of the eukaryotes, structural information is only available on *Plasmodium falciparum* GK, but GK is not essential for growth of the asexual blood stages in this organism (Schnick *et al.*, 2009). Kinetic studies also revealed a striking difference between the GKs of trypanosomes and those of other organisms (Kralova *et al.*, 2000). In *T. b. brucei* GK is encoded by five identical tandemly arranged genes (Colasante *et al.*, 2006) and plays an essential role in the survival of the parasite, especially in the absence of oxygen or in the presence of TAO inhibitors (Minagawa *et al.*, 1997), owing to its ability to catalyze the reverse reaction leading to the production of ATP required by the parasites. One may wonder whether the ability of the trypanosomal GK to catalyze the reverse reaction, in contrast to the human enzyme, is purely a consequence of the compartmentalization in glycosomes of the former or whether structure-based catalytic differences also make a contribution. We therefore perceive the parasite GK to be an interesting subject for structural investigation in terms of fundamental enzymology as well as drug-target exploitation. Here, we report the preliminary X-ray diffraction analysis of GK from *T. b. gambiense*, which may lead us to the design of parasite-specific GK inhibitors that spare the host enzyme. Since *T. b. brucei* TAO has also been crystallized recently (Kido *et al.*, 2010), X-ray structure analysis of both enzymes will aid us in the search for a new generation of chemotherapeutic agents against BSFs.

2. Materials and methods

2.1. Cloning and expression of TbgGK

Complementary DNA (cDNA) libraries were prepared from stocks of the bloodstream forms of *T. b. gambiense* (IL2343) and *T. b. rhodesiense* (Tbr; IL1501J21) using Toyobo reverse transcriptase. The cDNAs served as templates for the amplification of their GK-encoding genes (*gk*) by PCR using 5′-CACCATGAAGTACGTCGGATCCATT-3′ and 5′-CTACAACTTTGCCCACTTCGTCCTC-3′ as forward and reverse primers, respectively, with *PfuUltra* II Fusion HS DNA polymerase (Stratagene). The amplicons were gel-purified using the Toyobo gel-purification method. Plasmid constructs were obtained by cloning the blunt-ended gene into the pET151/D-TOPO plasmid vector (Invitrogen) by a ligation-independent cloning procedure. Cloning in this vector leads to the addition of an N-terminal tag containing a His_6 sequence, a V5 epitope and a tobacco etch virus (TEV) protease cleavage site (for removal of the fused 4 kDa tag) to the expressed recombinant protein.

One Shot TOP10 *Escherichia coli* cells were transformed with the Tbg or Tbr *gk*-pET151/D-TOPO plasmid construct by heat shock. Colonies were grown on Luria–Bertani (LB) plates containing 100 μg ml^{-1} carbenicillin and positive clones carrying the inserted gene were confirmed by colony PCR and selected for liquid culturing in LB media for construct amplification. Plasmid extraction from the cultured TOP10 cells was achieved using a Toyobo MagExtractor kit and was subjected to further confirmation by a combination of nested PCR and digestion with *Nco*I. Gene sequencing using the construct and designed sequencing primers was conducted using the dye-terminator method with an ABI Prism310 genetic analyzer (Applied Biosystems). The nucleotide sequence of *gk* revealed that the Tbg and Tbr GKs were exactly identical at the protein level; hence, Tbg *gk* was picked and used in this study. The recombinant plasmid was transformed into the JM109 (DE3 + pRARE2) *E. coli* strain (Novagen) for protein expression. Colonies of the transformants grown on an LB plate containing 100 μg ml^{-1} carbenicillin and 50 μg ml^{-1} chloramphenicol were selected and grown aerobically in LB medium containing the same concentrations of antibiotics.

The expression conditions were optimized for the amount and the activity of GK in the cytosolic fractions using activity measurements and SDS–PAGE by varying the concentration of the expression inducer isopropyl β-D-1-thiogalactopyranoside (IPTG), the temperature and the post-induction time before transformant harvest. The best yield was achieved with 25 μ*M* IPTG, growth at 293 K and post-induction for 8 h.

2.2. Assay of GK activity

The TbgGK activity was assayed using the reverse reaction of TbgGK (glycerol 3-phosphate + ADP → glycerol + ATP). To 1.0 ml of the reaction mixture (1 m*M* EDTA, 5 m*M* $MgSO_4$, 0.5 m*M* $NADP^+$, 50 m*M* glucose, 2 m*M* ADP, 10 m*M* glycerol 3-phosphate and one unit of hexokinase and glucose-6-phosphate dehydrogenase), TbgGK was added at 300 K. Using the ATP produced by TbgGK, hexokinase converts glucose to glucose 6-phosphate and finally glucose-6-phosphate dehydrogenase produces NADPH from glucose 6-phosphate and $NADP^+$. The rate of NADPH accumulation was spectrophotometrically monitored at 340 nm using a Jasco V-660 spectrophotometer.

2.3. Purification of recombinant TbgGK

For large-scale preparation, the transformant was grown at 293 K in 10 l LB medium for 8 h after induction and was harvested by centrifugation at 10 000*g*. The *E. coli* pellet was washed twice in 50 m*M* Tris–HCl buffer pH 7.6 containing 0.1 m*M* phenylmethylsulfonyl fluoride (PMSF) and was resuspended in 300 ml lysis buffer [100 m*M* phosphate buffer pH 6.8, 300 m*M* NaCl, 10 m*M* $MgSO_4$, 0.1 m*M* PMSF, 1 mg ml^{-1} lysozyme and 10%(*v*/*v*) glycerol]. The cell suspension was kept on ice for 30 min, passed twice through a French pressure cell operated at 140 MPa to break the cells and then subjected to centrifugation at 26 000*g* to remove unbroken cells and inclusion bodies. The supernatant was further centrifuged at 146 000*g* to remove residual undissolved material and then applied onto an Ni–NTA Agarose column (Qiagen; 1.5 × 15 cm) pre-equilibrated with 100 m*M* phosphate buffer pH 6.8 containing 20 m*M* imidazole, 300 m*M* NaCl, 10 m*M* $MgSO_4$ and 1%(*v*/*v*) glycerol. After washing the column with 100 ml of the same buffer, rTbgGK was eluted with 500 ml of buffer containing a linear gradient of 20–500 m*M* imidazole. Fractions containing active rTbgGK of higher purity as assessed

by SDS–PAGE (Laemmli, 1970) were pooled, concentrated to approximately 40 mg ml^{-1} using a centrifugal ultrafiltration tube (Amicon Ultra-15, 30 kDa cutoff; Millipore) and stored at 253 K in the presence of 50%(*v*/*v*) glycerol until the next purification step. About 5 mg of the affinity-purified protein was further purified by gel-filtration chromatography using a Superdex 200 (1 × 30 cm) column (GE Healthcare Biosciences) equilibrated with 100 m*M* phosphate buffer pH 6.8 containing 0.3 *M* NaCl and 1%(*v*/*v*) glycerol. Elution was carried out at a flow rate of 0.5 ml min^{-1} on a high-performance liquid-chromatography (HPLC) instrument. Each fraction (0.5 ml) was analyzed by SDS–PAGE and fractions containing highly pure rTbgGK were pooled. After buffer exchange to 10 m*M* MOPS buffer pH 6.8, 10 m*M* $MgSO_4$ and 1%(*v*/*v*) glycerol, the purified rTbgGK was concentrated to about 10 mg ml^{-1} for crystallization experiments. The addition of $MgSO_4$ and glycerol was crucial for preservation of the rTbgGK activity. The concentration of rTbgGK was estimated using the calculated molar extinction coefficient at 280 nm (ε_{280} = 81 080), giving an A_{280} of 1.0 for the pure rTbgGK solution at 0.74 mg ml^{-1}.

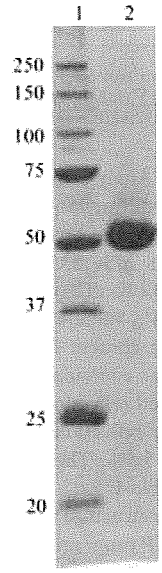

Figure 1
12.5% SDS–PAGE gel stained with Coomassie Brilliant Blue R-250 showing the apparent homogeneity of the purified rTbgGK. Lane 1, molecular-weight markers (kDa); lane 2, rTbgGK purified by Ni–NTA affinity chromatography and Superdex 200 gel filtration.

2.4. Crystallization and X-ray diffraction data collection

Crystallization conditions were initially screened at 277 and 293 K using the sitting-drop vapour-diffusion method in a 96-well Corning CrystalEX microplate with conical flat bottom (Hampton Research). A 0.5 µl droplet containing about 10 mg ml^{-1} rTbgGK dissolved in 10 m*M* MOPS buffer pH 6.8, 10 m*M* $MgSO_4$ and 1%(*v*/*v*) glycerol was mixed with an equal volume of reservoir solution and the droplet was allowed to equilibrate against 100 µl reservoir solution. In the initial screening experiment, commercially available screening kits from Hampton Research (Crystal Screen, Crystal Screen II, Grid Screen Ammonium Sulfate, Grid Screen PEG 6000, Grid Screen MPD and Quick Screen) and from Emerald BioStructures (Wizard Screen I and II) were used as the reservoir solutions. However, most of the conditions gave only heavy protein precipitates and the screening was unsuccessful. Screening was then carried out using a 5 mg ml^{-1} rTbgGK solution and twice-diluted reservoir solutions. Out of 290 conditions screened, tiny crystals and their aggregates appeared at 277 and 293 K from reservoir solutions containing 2.5–5%(*w*/*v*) PEG 6000 in the pH range 6.0–8.0. The conditions were further optimized by varying the buffer pH (5.6–8.4), the molecular weight of the PEG and its concentration [1–10%(*w*/*v*) for PEG 3350 and PEG 6000; 10–30%(*w*/*v*) for PEG 400]. Finally, single crystals suitable for X-ray diffraction experiments were obtained using a reservoir solution consisting of 30%(*w*/*v*) PEG 400 and 100 m*M* HEPES pH 7.0 within 24 h.

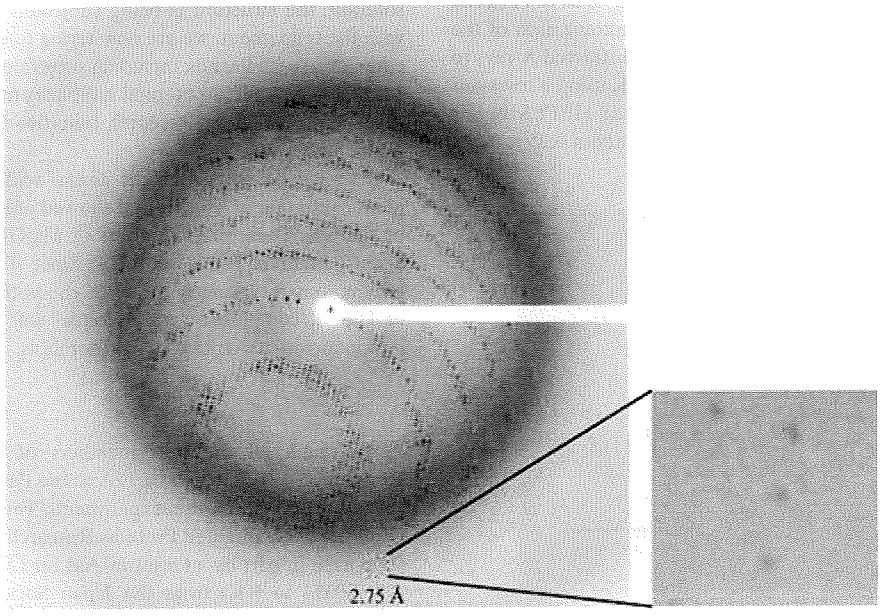

Figure 2
A typical X-ray diffraction pattern of an rTbgCK crystal. The detector edge corresponds to 2.4 Å resolution and an enlarged image of the indicated area around 2.75 Å resolution is shown. The exposure time was 1 s, with an oscillation angle of 1.0°.